Biogeosciences, 17, 5883–5908, 2020
https://doi.org/10.5194/bg-17-5883-2020

Biogeosciences Open Access EGU

Monsoonal forcing of cold-water coral growth off southeastern Brazil during the past 160 kyr

André Bahr[1], Monika Doubrawa[1,2], Jürgen Titschack[3,4], Gregor Austermann[1], Andreas Koutsodendris[1], Dirk Nürnberg[5], Ana Luiza Albuquerque[6], Oliver Friedrich[1], and Jacek Raddatz[7]

[1]Institute of Earth Sciences, Heidelberg University, Im Neuenheimer Feld 234, 69120 Heidelberg, Germany
[2]Earth and Environmental Sciences, KU Leuven, Celestijnenlaan 200e, 3001 Leuven, Belgium
[3]MARUM – Center for Marine Environmental Sciences, University of Bremen, Leobener Str. 8, 28359 Bremen, Germany
[4]Senckenberg am Meer, Marine Research Department, 26382 Wilhelmshaven, Germany
[5]GEOMAR Helmholtz Centre for Ocean Research, Wischhofstraße 1–3, 24148 Kiel, Germany
[6]Departamento de Geoquímica, Universidade Federal Fluminense, Outeiro São João Baptista s/n. – Centro, Niterói, RJ, Brazil
[7]Institute of Geosciences, Goethe University, Frankfurt, Altenhöferallee 1, 60438 Frankfurt am Main, Germany

Correspondence: André Bahr (andre.bahr@geow.uni-heidelberg.de)

Received: 3 June 2020 – Discussion started: 30 June 2020
Revised: 23 September 2020 – Accepted: 10 October 2020 – Published: 1 December 2020

Abstract. Cold-water corals (CWCs) constitute important deep-water ecosystems that are under increasing environmental pressure due to ocean acidification and global warming. The sensitivity of these deep-water ecosystems to environmental change is demonstrated by abundant paleorecords drilled through CWC mounds that reveal characteristic alterations between rapid formation and dormant or erosive phases. Previous studies have identified several central parameters for driving or inhibiting CWC growth such as food supply, oxygenation, and the carbon saturation state of bottom water, yet there are still large uncertainties about the relative importance of the different environmental parameters. To advance this debate we have performed a multiproxy study on a sediment core retrieved from the 25 m high Bowie Mound, located at 866 m water depth on the continental slope off southeastern Brazil, a structure built up mainly by the CWC *Solenosmilia variabilis*. Our results indicate a multifactorial control on CWC growth at Bowie Mound during the past ∼ 160 kyr, which reveals distinct formation pulses during northern high-latitude glacial cold events (Heinrich stadials, HSs) largely associated with anomalously strong monsoonal rainfall over the continent. The ensuing enhanced runoff elevated the terrigenous nutrient and organic-matter supply to the continental margin and likely boosted marine productivity. The dispersal of food particles towards the CWC colonies during HSs was facilitated by the highly dynamic hydraulic conditions along the continental slope that prevailed throughout glacial periods. These conditions caused the emplacement of a pronounced nepheloid layer above Bowie Mound, thereby aiding the concentration and along-slope dispersal of organic matter. Our study thus emphasizes the impact of continental climate variability on a highly vulnerable deep-marine ecosystem.

1 Introduction

Cold-water corals (CWCs) are hotspots of biodiversity in the deep-sea (Roberts and Cairns, 2014), important constituents of the deep-water carbon cycle (Lindberg and Mienert, 2005; Titschack et al., 2009, 2015, 2016; White et al., 2012; Cathalot et al., 2015), and potent bioengineers due to their sediment-baffling capacity that allows for enormous sediment accumulation rates of up to 1500 cm kyr^{-1} during maximum CWC mound formation phases (Titschack et al., 2015; Wienberg and Titschack, 2017, Wienberg et al., 2018). Yet the impact of global climate change on CWC reefs and the associated ecosystems beneath them is poorly constrained because the factors driving or inhibiting their occurrence and the potential thresholds in their resilience to environmental change are still under debate (Hebbeln et al., 2019; Raddatz and Rüggeberg, 2019). Geological records reveal that coral

mounds typically exhibit distinct phases of formation, often intercalated by intermittent periods of nondeposition and/or potentially erosion, indicating a high sensitivity of CWCs to changing boundary conditions (e.g., Rüggeberg et al., 2005; Kano et al., 2007; Frank et al., 2011; Raddatz et al., 2014, 2016; Wienberg and Titschack, 2017; Wienberg et al., 2018).

The most common framework-forming CWCs comprise *Lophelia pertusa* (recently assigned to the genus *Desmophyllum* by Addamo et al., 2016), *Macropora oculata*, *Solenosmilia variabilis*, *Bathelia candida*, and *Enallopsammia profunda* (e.g., Mangini et al., 2010; Frank et al., 2011; Muñoz et al., 2012; Hebbeln et al., 2014; Raddatz et al., 2020). Field and laboratory studies of *L. pertusa*, the most intensively investigated species, suggest that scleractinian CWCs are nonspecialists regarding food sources, which range from particulate to dissolved organic carbon (POC and DOC, respectively; Kiriakoulakis et al., 2005; Duineveld et al., 2007; Gori et al., 2014; van Oevelen et al., 2016), algae, bacteria, and zooplankton (Gori et al., 2014; Mueller et al., 2014). However, we note that similar studies on the feeding preferences of *S. variabilis*, the dominant framework-building CWC at the herein investigated Bowie Mound (Raddatz et al. 2020), are still missing. Additionally, changes in the properties and spatial configuration of ambient intermediate- or deep-water masses may also strongly impact CWCs through changes in the dissolved oxygen concentration and the seawater parameters pH, alkalinity, and carbonate-ion concentration. All these parameters affect the capacity of CWCs to build their aragonitic framework (e.g., Form and Riebesell, 2012; Maier et al., 2012; Lunden et al., 2014; Hennige et al., 2015; Büscher et al., 2017; Auscavitch et al. 2020). Spatial fluctuations of intermediate- to deep-water masses further influence the depth and strength of pycnoclines, which are thought to play an important role in the concentration and dispersal of nutrients and food utilized by CWCs (Frederiksen et al., 1992; Duineveld et al., 2007; Mienis et al., 2007; Rüggeberg et al., 2016). Aside from processes directly affecting the water-mass properties bathing CWCs, several studies also point to the importance of sea surface productivity in providing food to the deep ocean (Davies et al., 2009; Soetaert et al., 2016). However, despite the proximity of CWC mounds situated on the continental slope to adjacent continents, the role of terrestrial nutrient and POC input is still a matter of debate (Wienberg et al., 2010; Hanz et al., 2019; Fentimen et al., 2020).

To systematically test the relative importance of the diverse factors potentially influencing CWC growth and mound formation, we investigated the response of CWCs at Bowie Mound, a coral-bearing mound in the Campos Basin on the continental slope offshore southeastern Brazil (Bahr et al., 2016; Raddatz et al., 2020), to changes in paleoenvironmental conditions. The presence of CWC-bearing mounds off Brazil was first reported by Viana et al. (1998) and Sumida et al. (2004) along the continental slope at intermediate water depths, between 500 and 1000 m, bathed by Antarctic Intermediate Water (AAIW). At Bowie Mound, the dominating species is *S. variabilis*, which is adapted to colder (as low as 3–4 °C; Fallon et al., 2014; Flögel et al., 2014; Gammon et al., 2018) and less aragonite-saturated waters than *L. pertusa* (Thresher et al., 2011; Flögel et al., 2014; Bostock et al., 2015; Gammon et al., 2018).

The selected location at Bowie Mound is ideally suited to assess a variety of external factors capable of driving CWC growth dynamics as it is situated at the interface of distinctly different water masses (cf. Sect. 2) and is strongly influenced by terrigenous input from land and the broad shelf off Cabo Frio, which experiences intense seasonal upwelling. This setting allows us to test the relative importance of different factors that are potentially crucial for the CWC growth at Bowie Mound, in particular (i) intermediate water-mass variability via its impact on nutrient (e.g., Fe, P, N) concentration, food availability, and local hydrodynamics and (ii) variations in nutrient and organic-matter fluxes derived from upwelling and terrestrial input in the context of global climatic changes. Our unique set of multiproxy data combined with Th/U-dated CWCs demonstrates that an invigorated continental hydroclimate played a thus far underestimated role in triggering CWC growth at the southeastern Brazilian margin – a scenario that is likely affecting CWC mounds worldwide.

2 Hydrological, climatological, and geological setting

The (sub)surface circulation in the western tropical South Atlantic at the Campos Basin off southeast Brazil is dominated by the southward-flowing, warm Brazil Current (BC; Fig. 1). The BC forms the western portion of the anticyclonic subtropical gyre (Stramma and England, 1999), which is characterized by high evaporation rates that produced the Salinity Maximum Water (SMW; 24 °C, $\sigma_\theta \sim 25.2$) in the upper 200 m of the water column. The interaction of the BC with the coastal hydrographic system promotes subsurface upwelling of South Atlantic Central Water (SACW) on the shelf edge and on the shelf (Roughan and Middleton, 2002; Aguiar et al., 2014). Upwelling is particularly strong during austral spring and summer, when northeasterly winds generate upward Ekman pumping on the mid shelf (Castelao and Barth, 2006; Castelao, 2012), which fuels productivity due to the subsurface encroachment of nutrient-rich SACW. The SACW is found from below the SMW up to 500 m water depth and is characterized by decreasing temperatures and salinities (20 °C, 36.0 psu to 5 °C, 34.3 psu; Fig. 1; Raddatz et al., 2020) owing to its formation in the southwest Atlantic and the southern Indian Ocean (Sverdrup et al., 1942; Stramma and England, 1999). The AAIW (34.3 PSU, ∼ 4 °C; Fig. 1) lies below the SACW and above North Atlantic Deep Water (NADW), which is present below 1100 m water depth and has higher oxygen concentrations and salinities compared to AAIW (Mémery et al., 2000). Below ∼ 2500 m the Antarctic Bottom Water (AABW) constitutes the deepest and

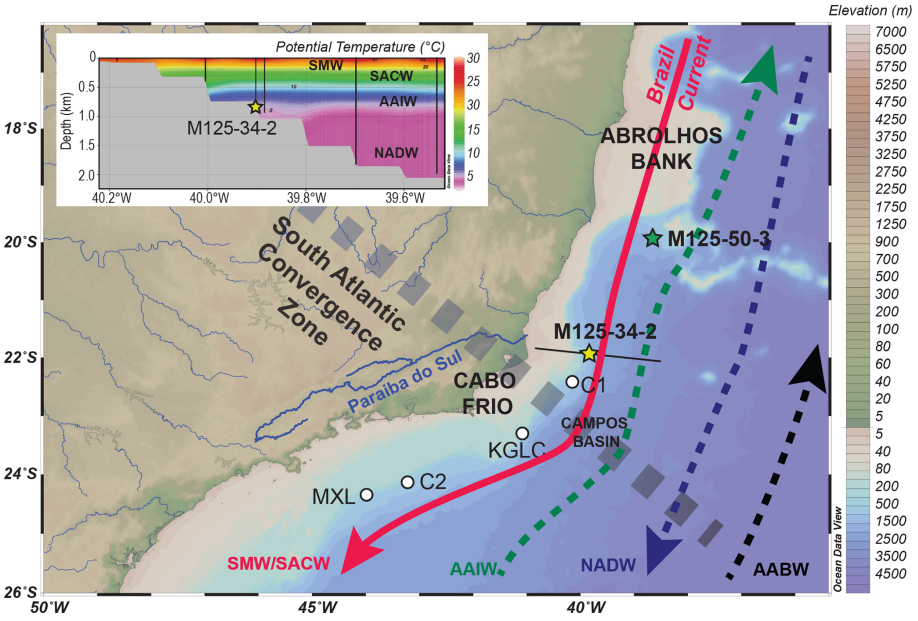

Figure 1. Location of core M125-34-2 (yellow star) on Bowie Mound, reference core M125-50-3 (green star) and other CWC records published in Mangini et al. (2010) and Ruckelshausen (2013; white dots). Major surface- (red line), intermediate- (green), and deep-water circulation features (blue) and water masses are indicated as well as the approximate location of the South Atlantic Convergence Zone (stippled line) as the main atmospheric feature. The inset shows a hydrographic section crossing the location of Bowie Mound core M125-34-2 with potential temperatures as measured via CTD (black lines) during R/V *METEOR* expedition M125 (Bahr et al., 2016; Raddatz et al., 2020); the location of the hydrographic section is indicated by a black line on the map. Figure modified after Raddatz et al. (2020). AABW: Antarctic Bottom Water; AAIW: Antarctic Intermediate Water; NADW: North Atlantic Deep Water; SACW: South Atlantic Central Water; SMW: Salinity Maximum Water.

most dense water mass in this region (Stramma and England, 1999).

The interaction between the northward- or southward-directed flow of the different water masses with the morphology of the slope at Campos Basin forms strong geostrophic currents (Viana and Faugères, 1998; Viana et al., 1998; Viana, 2001). These currents are responsible for enhanced sediment focusing, leading to the formation of drift bodies, while internal waves at the boundary between different water masses create widespread erosional surfaces (Viana et al., 1998; Viana, 2001).

Bowie Mound itself has a total elevation of 25 m and is situated within a field of mound-like structures, which are presently barren of living framework-forming CWCs (Bahr et al., 2016). Located at 866 m water depth, it lies within the core of the AAIW. Hence, it can be expected that changes in the nutrient and organic-matter inventory of the AAIW (Poggemann et al., 2017) and/or displacement of the intermediate water mass may have had a direct impact on the hydrodynamic conditions at Bowie Mound.

The Campos Basin receives freshwater and sediment input primarily from the Paraíba do Sul river, which delivers between 180 and 4400 $m^3\ s^{-1}$ of water (Carvalho et al., 2002) and 30 $t\ yr^{-1}$ of sediment (Jennerjahn et al., 2010) to the study area. Most precipitation in the hinterland of the Paraíba do Sul river occurs during austral summer, when strong atmospheric convection forms the South Atlantic Convergence Zone, an elongated band of heavy precipitation that reaches from central Amazonia into the tropical South Atlantic (Carvalho et al., 2004; Marengo et al., 2012; Fig. 1).

3 Material and methods

3.1 Material

Gravity core M125-34-2 was retrieved during R/V *METEOR* cruise M125 from the top of the 25 m high Bowie Mound at 866 m water depth at 21°56.957′ S and 39°53.117′ W (exact positioning was secured by the Ultra-Short-Baseline system POSIDONIA; Fig. 1; Bahr et al., 2016). The core was cut into 1 m segments onboard and stored unopened at −20 °C. After CT scanning, the core was opened in the frozen state (for details on the CT scanning see Skornitzke et al., 2019; Raddatz et al., 2020). Discrete samples for X-ray diffractometry (XRD), grain-size analyses, C and N content, and stable-carbon- and stable-oxygen-isotope analyses of foraminifera and organic matter were taken from the sediment matrix, avoiding the sampling of coral fragments. X-ray fluorescence (XRF) scanning was performed on the archive halves while

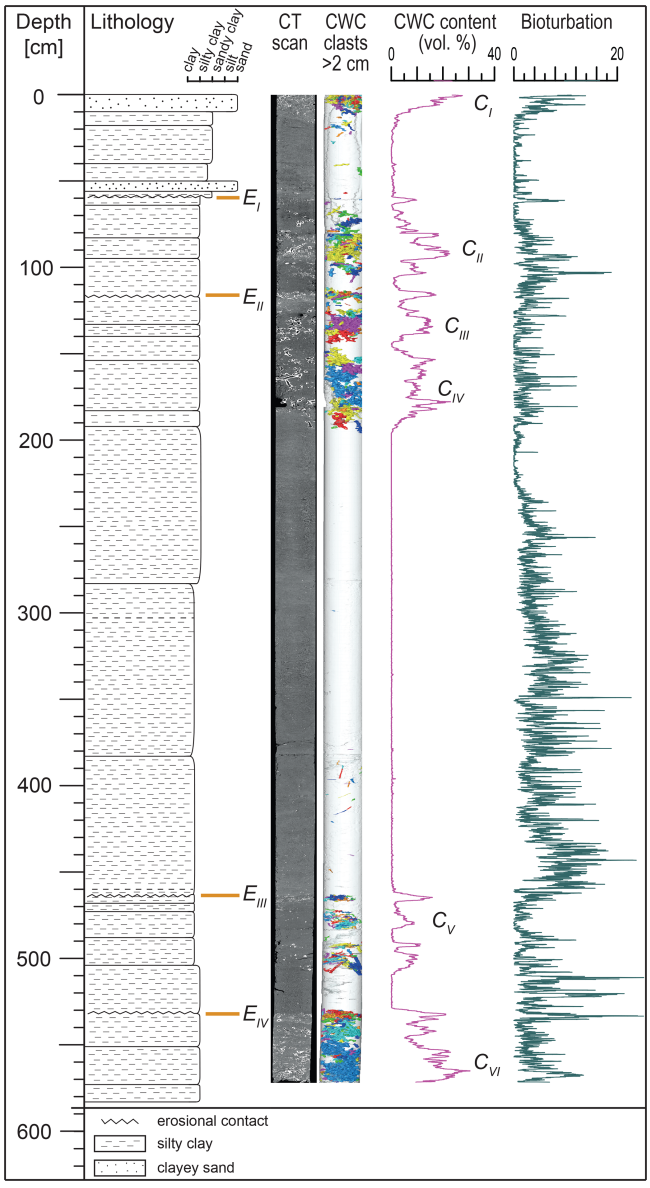

Figure 2. Lithological log of core M125-34-2 (21°56.957′ S, 39°53.117′ W; 866 m water depth) including CT-scanning image and CWC clasts > 2 cm, CWC content, and bioturbation index. Erosional surfaces E_I–E_{IV} are indicated as well as CWC-bearing intervals C_I–C_{VI} after Raddatz et al. (2020).

avoiding coral segments when defining the sampling path of the detector.

Core M125-34-2 (Fig. 2) consists of moderately to strongly bioturbated olive-gray to dark-gray, silty clayey sand with alternating coral-bearing and coral-free zones (Raddatz et al., 2020). The sediments are rich in micro- and macrofossils, including pteropods and bivalves as well as benthic and planktonic foraminifers. Six intervals (C_I–C_{VI}) of particularly high coral contents of up to 31 vol. % were identified within the core at 0–13, 80–105, 131.5–138, 157–190, 479.5–480.5, and 549.5–568 cm (Fig. 2; Raddatz et al., 2020). Coral-bearing intervals are characterized by the presence of *S. variabilis* and to a minor degree *M. oculata* as the major macrofossils (clast length > 2 cm). Visual inspection and CT imaging (Appendix Figs. A–F) reveal four prominent erosive surfaces (E_I–E_{IV}) with abundant coral fragments and shell debris at 58, 117, 465, and 532 cm (Fig. 2).

To constrain the chronostratigraphy of core M125-34-2 and to assess the intermediate-water variability, adjacent core M125-50-3 (19°56.957′ S, 38°35.979′ W; 904 m water depth; Fig. 1) was sampled at 10 cm intervals for $\delta^{18}O$ analyses. Core M125-50-3 is barren of CWCs and consists of bioturbated, greenish-gray hemipelagic mud with darker and lighter intervals. Two sandy, foraminifera-rich layers at 1226 and 1230 cm might point to periods of condensed sedimentation; otherwise no unconformities or erosive surfaces could be identified.

3.2 Quantitative analysis of CT-scanning data

Prior to opening, the sediment core sections were scanned with a SOMATOM Definition Flash computer tomograph at the Clinic of Diagnostic and Interventional Radiology (DIR) of Heidelberg University Hospital, Heidelberg, Germany, with 140 kVp tube potential and 570 mAs tube current – time product with a pitch of 0.4 (for details see Skornitzke et al., 2019). The raw data with a resolution of 0.5 mm in z orientation and 0.3 mm in xy orientation were reconstructed iteratively (ADMIRE, Siemens Healthineers) using a sharp kernel (I70 h level 3) to an isotropic voxel size of 0.35 mm. Further data processing was carried out with the ZIB edition of the Amira software (Stalling et al. 2005; http://amira.zib.de, last access: 16 November 2020). Within Amira, the core sections were virtually reunited, and the core liner and marginal coring artifacts were removed (∼2 mm of the core rim). Furthermore, coral clasts were segmented and separated with the ContourTreeSegmentation module (threshold: 1400; persistence value: 1150) and quantified. Macrofossils > 2 cm were visualized as surfaces in 3D following the methodology of Titschack et al. (2015). As an index for bioturbation, we determined the standard deviation of the matrix sediment X-ray attenuation within each XY-oriented CT slice. The matrix sediment was segmented by selecting the data volume surrounding the corals, removing areas with values < 500 HU (considered to represent air and water) and reducing the remaining segmented volume by three voxels to avoid marginal artifacts in the X-ray attenuation caused for example by the resolution-dependent averaging effect.

3.3 X-ray fluorescence (XRF) scanning

XRF core scanning was performed on the archive halves of the split core. All segments of core M125-34-2 were scanned at Heidelberg University using an Avaatech (GEN4) XRF core scanner. XRF core scanner data were collected every

1.0 cm down-core with a 1.2 cm cross-core slit size. The split core surface was cleaned and covered with a 4 µm thin SPEX-Certi Prep Ultralene1 foil to avoid contamination of the XRF measurement unit. Core intervals with very abundant corals were skipped to avoid damage of the foil covering the detector through sharp and rigid edges of coral fragments. Data were collected in two separate runs using generator settings of 10 and 30 kV and currents of 0.2 and 1.0 mA, respectively. Sampling time was set to 20 s per measurement. To counteract artifacts derived from variations in sediment porosity, water content and surface roughness as well as element counts were normalized by dividing the value of the component (C) by the sum of the counts for each depth (Bahr et al., 2014).

3.4 X-ray diffractometry (XRD)

About 9 g of wet material was dried in an oven at 40 °C and subsequently milled in a ball mill (Pulverisette, FRITSCH) with 300 cycles per second for 3 min to obtain a powder with a grain size of 1–3 µm. The XRD measurements were carried out at the Institute of Earth Sciences, Heidelberg University, using a Bruker D8 ADVANCE Eco diffractometer (40 kV, 25 mA) with a Cu Kα diode. The samples were measured in rotating, circular, synthetic sample holders. An angular range of 2θ from 5 to 70° was measured with a step size of 0.02 increments (3338 steps per sample) for 1 s per step. Peak positions and intensity of data were analyzed with Diffrac.Suite EVA (Bruker Software). The Rietveld refinement program DIFFRAC.TOPAS (Bruker Software) was used to perform quantitative phase analysis.

3.5 Grain-size analysis (sortable silt, $\overline{\text{SS}}$)

The preparation of the samples for the $\overline{\text{SS}}$ analyses followed Bianchi et al. (2001) and Stuut et al. (2002). Wet samples with a weight between 0.3 and 1 g were dried over night at 40 °C. Macroscopically visible coral fragments were removed. After weighting the dry samples, 10 mL of 30 % H_2O_2 was added to each sample to dissolve the organic material under sub-boiling conditions on a heating plate until the reaction ceased. To remove carbonates, 5 mL HCl (10 %) was added to each sample under sub-boiling conditions for at least 10 min until the end of the reaction. Samples were washed through standard sieves (63 µm mesh size) to remove the sand and coarser fraction. The fraction > 63 µm was dried at 40 °C and weighed. The material < 63 µm was transferred into 1 L beakers and filled to the top with demineralized water. After a settling period of at least 8 h, the supernatant water was decanted and the sample transferred into a 200 mL beaker, topped with demineralized water and left to settle for 8 h. After decanting supernatant water, the samples were transferred into 50 mL plastic beakers and put into an ultrasonic bath to disintegrate aggregated sediment particles. Afterwards, 35 mL Na pyrophosphate was added to prevent particles from forming new aggregates, and 2 mL isopropyl alcohol was added to minimize the formation of air bubbles in the liquid. Samples were measured with a laser particle sizer (LPS) ANALYSETTE 22 by FRITSCH™ at the Institute of Earth Sciences, Heidelberg University, in wet dispersion covering the range 0.08–2000 µm with 99 size classes. The raw data were analyzed with the software MaScontrol (FRITSCH™) by applying a Fraunhofer model. Results are derived from a total of five analytical runs with 100 scans per sample. Up to seven replicate samples were performed for each depth to minimize the natural variability of the samples. While there is relatively large intersample variability that is likely caused by the high number of mica flakes present in the sediment, distorting the laser beam, we nevertheless consider the results retrieved via the ANALYSETTE 22 to be reliable (for an in-depth discussion see Jonkers et al., 2009).

3.6 Carbon and nitrogen content

Sediment samples were homogenized with a mortar and pestle and then weighted (0.5 mg for each analyses). The total organic carbon (TOC) and inorganic carbon (TIC; together TC) content was analyzed with a LECO RC-412 (Institute of Geoscience, Goethe University Frankfurt). The reproducibility of the replicate analyses was < 0.1 %. The total nitrogen (TN) content was analyzed with a LECO TruSpec Macro (Institute of Geoscience, Goethe University Frankfurt).

3.7 Stable-oxygen and stable-carbon analysis

3.7.1 Stable-isotope analysis of foraminiferal calcite

For stable-isotope analyses of core M125-34-2, samples were taken at 5–10 cm intervals, wet-sieved (> 63 µm), and then dried. For each sample, one to three tests of *Uvigerina* spp. (*U. peregrina* and *U. proboscidea*) or *Planulina wuellerstorfi* were selected from the size fraction > 125 µm, depending on availability. Stable-carbon- and stable-oxygen-isotope ratios were measured on a Thermo Fisher MAT 253 Plus IRMS gas isotope ratio mass spectrometer with a coupled Kiel IV automated carbonate preparation device at the Institute of Earth Sciences, Heidelberg University. The instrument was calibrated using the in-house standard (Solnhofen limestone), which is calibrated against the IAEA-603. Values are reported versus the VPDB (Vienna Pee Dee Belemnite) standard. Standard deviations derived from repeated measurements of the internal standard are ± 0.06 ‰ for stable oxygen isotopes (δ^{18}O) and ± 0.03 % for stable carbon isotopes (δ^{13}C).

The ∼ 13 m long core M125-50-3 was sampled every ∼ 10 cm for benthic-foraminiferal-isotope analysis. The samples were freeze-dried and washed through a > 63 µm sieve to separate the coarse and fine fractions. Specimens of the benthic genera *Uvigerina* spp. were hand-picked from the size fraction 315–400 µm. δ^{18}O analyses were performed on a Thermo Scientific MAT 253 mass spectrometer with an au-

tomated Kiel IV carbonate preparation device at GEOMAR. The isotope values are calibrated versus the NBS19 (National Bureau of Standards) carbonate standard and the in-house "Standard Bremen" (Solnhofen limestone). Isotope values presented in the delta notation are reported in permil (‰) relative to the VPDB scale. The analytic error is ± 0.06 ‰ for δ^{18}O and ± 0.03 ‰ for δ^{13}C.

3.7.2 Stable-isotope analysis of organic matter

Previously homogenized samples were decarbonized with 10 % HCl to remove all inorganic carbon. Afterwards, the samples were centrifuged and washed several times with deionized water in order to remove residual HCl. The samples were then dried in an oven at 50 °C. Subsequent analyses of the carbon isotopic composition of organic carbon ($\delta^{13}C_{org}$) were performed by a Flash Elemental Analyzer 1112 connected to the continuous-flow inlet system of a MAT 253 gas source mass spectrometer (Institute of Geosciences, Goethe University Frankfurt). Samples and standards both reproduced within ± 0.2 ‰ and are reported relative to the VPDB standard.

3.8 Statistical analysis

Correlation coefficients and associated p-values were calculated using the Monte-Carlo-based SurrogateCorr function implemented in the "astrochron" package in R (Meyers, 2014) with 1000 iterations. This method was developed particularly to assess the correlation of parameters sampled at different down-core resolutions (e.g., XRF scanning data vs. discrete grain-size measurements; Meyers, 2014).

Discriminant analysis was performed with the program PAST (v3.15; Hammer et al., 2001). Prior to analysis, the data were detrended and normalized to the mean and standard deviation.

4 Age model refinement

The age model of core M125-34-2 used in this study represents a refined version of the stratigraphy published in Raddatz et al. (2020), which is based on ^{230}Th/U dates of CWCs. The six coral-bearing intervals, as described in Sect. 3.1, exhibited a mean accumulation rate of 30 cm kyr^{-1} with an overall range from 2 cm kyr^{-1} (C_V) to 80 cm kyr^{-1} (C_{III}; Raddatz et al., 2020).

To better constrain the age of CWC-barren intervals and evaluate the chronostratigraphic duration of potential hiatuses, we compared the δ^{18}O record of core M125-34-2 with the benthic-isotope record of adjacent core M125-50-3. The clear glacial–interglacial pattern of $\delta^{18}O_{Uvi}$ in core M125-50-3 allows for the construction of a robust age model for this site by tuning its benthic-isotope record to the LR04 benthic stack (Lisiecki and Raymo, 2005) and indicates that it extends to $\sim$ 135 ka (Fig. 3). Its stratigraphic range is thus only slightly shorter than the one of M125-34-2 (158 ka based on Th/U dates) and is therefore suitable as an off-mound reference site. As both cores are situated in similar water depths and are thus bathed by the same water mass (today the AAIW; see Sect. 2), we expect the respective δ^{18}O values to not only follow a common glacial–interglacial pattern but also to be comparable in their absolute values, allowing for further constraining of the chronostratigraphy of M125-34-2.

As neither shallow infaunal *Uvigerina* spp. nor epibenthic *P. wuellerstorfi* was consistently present throughout core M125-34-2, we generated a spliced record of both species. For the δ^{18}O splice we corrected values of *P. wuellerstorfi* by adding the correction factor of +0.47 ‰ according to Marchitto et al. (2014). The resulting combined δ^{18}O record of M125-34-2 exhibits a considerable scatter from the top to erosive horizon E_I including relatively depleted $\delta^{18}O_{Plan}$ values as low as 2.5 ‰ (Fig. 3), which puts this interval into a transitional phase between glacial and interglacial δ^{18}O levels. Neither δ^{18}O values nor absolute dating support the preservation of Holocene deposits at the top of the gravity core. A deglacial age for the deposition of this interval is further corroborated by Th/U dates of 13.7 and 14.3 ka, respectively. Samples from between E_I and E_{II} show slightly heavier δ^{18}O values and Th/U dates clustering around 16.5 ka, which indicates a post-LGM (Late Glacial Maximum) deposition. The existing Th/U dates suggest that the hiatus represented by the erosive unconformity E_I is most likely shorter than 2 kyr. The section between E_{II} and E_{III} on the other hand has relatively uniform δ^{18}O values around 4.3 ‰ ($\delta^{18}O_{Uvi}$) and 3.4 ‰ ($\delta^{18}O_{Plan}$), respectively, which matches M125-50-3 $\delta^{18}O_{Uvi}$ values during MISs 4 to 2. A Th/U date at the top of this section at 117 cm reveals an age of 34 ka, while CWC ages from slightly deeper in the core (between 131 and 190 cm) fall within the range of 60–63 ka (MIS 4). As $\delta^{18}O_{Uvi}$ values between E_{II} and E_{III} are less depleted than MIS 5 samples of reference site M125-50-3, we infer that those sediments were most likely deposited during MIS 4 and did not reach into MIS 5. Hence, it appears that deposits of MIS 2 and large parts of MIS 3 are not present in core M125-34-2, either due to nondeposition or subsequent erosion (note the prominent erosive surface E_{II}). This age assignment would also imply that the extended CWC-free portion from 200 to 465 cm was deposited within a short period of approximately 8 kyr during MIS 4 (62.2 ka as the oldest Th/U dates and $\sim$ 70 ka as the MIS 4–5 boundary). This would yield a sedimentation rate of 33 cm kyr^{-1} (Fig. 3a), which is typical for contouritic sediments at the southeastern Brazilian margin (Viana et al., 1998; Hernández-Molina et al., 2014; Rebesco et al., 2014). The following interval between E_{III} and E_{IV} has relatively depleted $\delta^{18}O_{Uvi}$ values that fall into the range of MIS 5a–d values in reference core M125-50-3. Th/U dates of $\sim$ 107 ka for CWCs below E_{III} support a deposition during MIS 5d and further indicate a prolonged interval of nondeposition or erosion, leading to

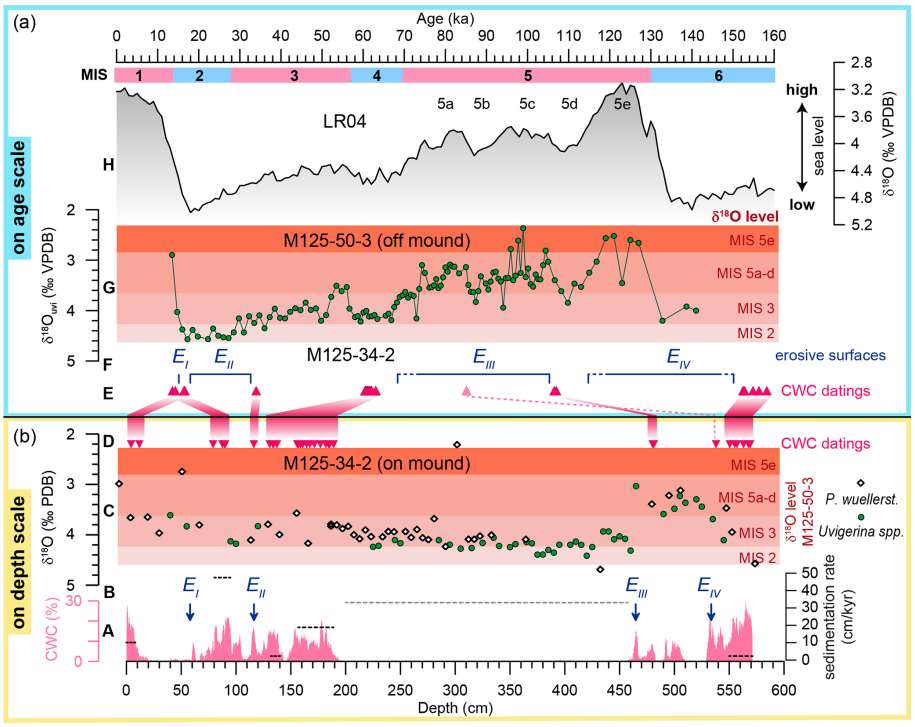

Figure 3. Refined age model of core M125-34-2 from Bowie Mound. Panel **(b)** displays data from M125-34-2 on depth scale, comprising **(A)** CWC abundances (%; magenta) based on CT scanning and accumulation rates for both the Th/U-dated CWC-bearing intervals (black dashed lines; cf. Raddatz et al., 2019) and the CWC-barren interval between 200 and 465 cm (dashed gray line); **(B)** blue arrows denote erosive horizons (hiatuses) E_{I}–E_{IV} (cf. Fig. 2); **(C)** benthic-δ^{18}O data from *Uvigerina* spp. (green dots) and *P. wuellerstorfi* (white diamonds; elevated by $+0.47$ to adjust for the interspecies offset to *Uvigerina* spp. after Marchitto et al., 2014); red horizontal shadings indicate reference δ^{18}O levels for the respective marine isotope stages (MISs) taken from off-mound core M125-50-3 (see **G**); **(D)** red triangles mark Th/U datings. Panel **(a)** displays data in the time domain with **(E)** Th/U dates of M125-34-2; **(F)** the inferred duration of hiatuses reflected by erosive horizons E_{I}–E_{IV} of core M125-34-2; **(G)** the δ^{18}O record on *Uvigerina* spp. in off-mound core M125-50-3, with red horizontal shadings illustrating the δ^{18}O level during different isotope stages as used in **(C)**; and **(H)** the LR04 benthic stack (Lisiecki and Raymo, 2005) as an approximation for eustatic sea-level changes. MISs are indicated by pink and blue bars, signifying relatively warm and cold periods, respectively.

the absence of MIS 5a–c in core M125-34-2. As δ^{18}O values below E_{IV} are again at glacial levels, this section can be assigned to MIS 6, which is in line with Th/U dates of 152.6–158.4 ka. Hence the penultimate interglacial MIS 5e is likely not recovered and falls into the hiatus represented by E_{IV}.

In summary, deposition at Bowie Mound site M125-34-2 appears to be concentrated during glacial intervals of intermediate ice volume and reduced during interglacial periods. The erosive horizons present in core M125-34-2 caused by winnowing due to strong current activity and internal waves provide evidence for extreme variability in the hydrological regime at the southeastern Brazilian margin (Viana and Faugères, 1998; Viana et al., 1998; Viana, 2001). While winnowing has the capacity to remove the sediment matrix, leading to lag deposits, it is rather unlikely that it would also remove coral fragments. Hence, it is feasible to assume that the dated intervals of CWC presence represent the complete sequence of CWC presence at this part of Bowie Mound.

5 Results and discussion

In the following we discuss if and how changes in environmental parameters might have enhanced or prohibited CWC growth at Bowie Mound, focusing on the role of intermediate water-mass variability and varying terrigenous-sediment supply. We argue that the most dominant environmental factor for triggering CWC growth was elevated river runoff during periods of strong monsoonal rainfall in the coastal hinterland, which provided nutrients and organic matter that enhanced the food supply of CWC colonies.

5.1 Drivers and inhibitors of CWC growth at Bowie Mound

5.1.1 Intermediate water-mass properties and hydraulic dynamics

Intermediate water-mass properties may have played a crucial role for the development of Bowie Mound. First, Bowie Mound lies within the AAIW, which probably boosted CWC growth at the eastern Brazilian slope. Secondly, nutrients and POC typically concentrate within nepheloid layers at water-mass boundaries and provide a prolific food source for CWCs (Mienis et al., 2007; Dullo et al., 2008; Raddatz et al., 2014; Rüggeberg et al., 2016; Magill et al., 2018). In the case of Bowie Mound, it is possible that enhanced production (Pahnke and Zahn, 2005; Pahnke et al., 2008) and/or nutrient-enrichment (e.g., increasing phosphate and nitrate concentration) of the AAIW (Poggemann et al., 2017) during phases of weak Atlantic Meridional Overturning Circulation (AMOC) could have triggered its episodic formation phases. A more prominent AAIW likely also strengthened internal waves hitting the slope at the AAIW–SACW boundary in the Campos Basin (Viana et al., 1998; Viana, 2001) and thus fueled the nepheloid layer by enhanced resuspension.

Here, we use the benthic δ^{13}C obtained in M125-34-2 as an indicator of the relative contribution of ^{13}C-depleted southern-sourced intermediate water masses (Kroopnick, 1985; Curry and Oppo, 2005). As we had to use different species (shallow infaunal *Uvigerina* spp. and epibenthic *P. wuellerstorfi*), we combined both records. To adjust for intraspecies offsets, we followed the approach of Kaboth et al. (2017) and normalized the δ^{13}C values of each species to the respective mean and standard deviation. The resulting normalized data exhibit a considerable scatter in the *Uvigerina* spp. record due to the pooling of different species and hence only allow for a discussion of major shifts in the isotopic composition. However, the δ^{13}C data of *Uvigerina* spp. and *P. wuellerstorfi* do not provide compelling evidence for distinctly depleted values during phases of CWC growth compared to CWC-barren intervals (Fig. 4). Although $\delta^{13}C_{\mathrm{Uvi}}$ might be influenced by isotopic variations in dissolved inorganic carbon of pore water (Zahn et al., 1986) and interspecies offsets (Rathburn et al., 1996; Theodor et al., 2016), we nevertheless consider it to be appropriate for reconstructing major changes in the bottom-water signature. Even when only considering $\delta^{13}C_{\mathrm{Plan}}$, there are no apparent systematic differences between CWC-bearing and CWC-barren intervals. The continuous, monospecific $\delta^{13}C_{\mathrm{Uvi}}$ record obtained in off-mound core M125-50-3 likewise lacks negative excursions during times of CWC growth at Bowie Mound (Fig. 5c). Hence, it appears that changes in the nutrient or organic-matter content of the AAIW as observed during the last deglaciation (Poggemann et al., 2017) did not significantly affect CWC growth.

While nutrient and/or food delivery by the AAIW seems to have had an insignificant effect on CWC growth at Bowie Mound, changes in the hydrodynamic regime affecting the depth and strength of the nepheloid layer might have had an impact on CWC proliferation. Hydrodynamic conditions at core M125-34-2 can be reconstructed by using the variation in $\overline{\mathrm{SS}}$, a well-established proxy for bottom-current speed reflected by the mean grain size of the 10–63 µm fraction (McCave et al., 1995) and the sedimentary ln(Zr/Al) ratio (Fig. 4). The latter proxy follows the rationale that heavy minerals accumulate relative to aluminosilicates when the bottom-current flow speed is high (e.g., Turnewitsch et al., 2004; Bahr et al., 2014; Miramontes et al., 2019). The significant correlation ($r = 0.49$, $p < 0.05$) of both proxies therefore predominantly reflects the hydraulic regime at Bowie Mound despite certain intervals where both parameters deviate (e.g., between 60 and 115 cm with high $\overline{\mathrm{SS}}$ and low ln(Zr/Al) values), which might be due to small-scale hydraulic effects created by the CWC branches themselves (Mienis et al., 2019). Based on both hydrodynamic proxies, CWCs at Bowie Mound tend to accumulate during intervals with elevated flow speed. Phases of low flow speed are accompanied by low CWC abundances (e.g., at 140–150 and 465–550 cm), in line with the notion that active bottom currents play a significant role in distributing nutrients and food towards CWC colonies (e.g., Thiem et al., 2006; Dorschel et al., 2007; Davies et al., 2009; Raddatz et al., 2011). High current speeds will also increase sediment supply, thereby increasing accumulation rates due to the baffling capacity of CWC. Our data, however, suggest that a relatively high flow speed does not necessarily lead to CWC growth, as demonstrated by the extended CWC-free section between 200 and 460 cm, where ln(Zr/Al) and $\overline{\mathrm{SS}}$ reach high levels, and at 15–60 cm, where no CWCs are preserved despite high TOC accumulation. Hence, the absence of CWCs, despite persistently high bottom-current speeds during most of the glacial intervals MISs 3 and 4, indicates that environmental drivers other than intermediate water-mass variability must have played an important role for triggering CWC proliferation on the Brazilian margin.

5.1.2 Terrestrial and marine organic-matter supply

Having a sufficient food supply to Bowie Mound is a prerequisite for enhanced CWC growth. To assess the potential impact of enhanced POC and/or DOC supply as an incentive for enhanced CWC growth, we compared TOC measurements to CWC abundances (Fig. 6). It appears that CWC abundance is highest during intervals of elevated organic-matter content, while the long CWC-barren interval between 200 and 460 cm is characterized by relatively low TOC contents, thus stressing the importance of TOC as a prerequisite for mound aggregation. While statistically significant, the down-core pattern of CWC abundances and TOC ($r = 0.55$, $p < 0.05$) also indicates that this correlation is not straightforward; an ex-

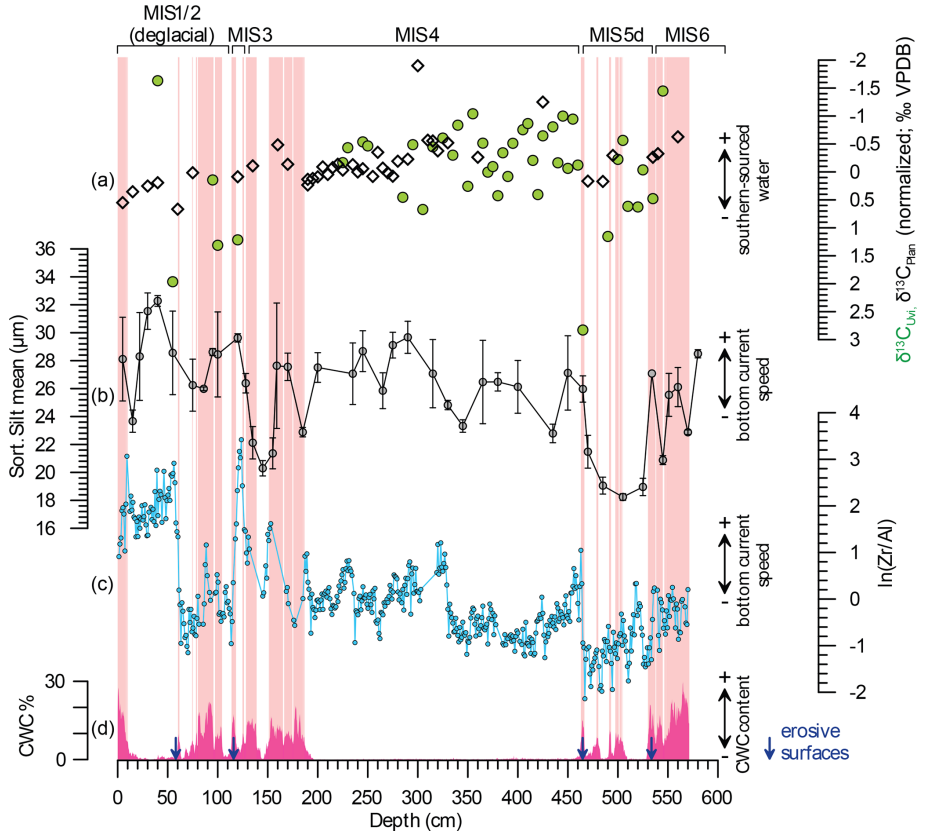

Figure 4. Proxies of intermediate water-mass variability vs. phases of mound formation obtained in core M125-34-2. **(a)** Normalized δ^{13}C of *Uvigerina* spp. (green dots) and *P. wuellerstorfi* (white diamonds) as a proxy for bottom-water-mass origin; **(b)** mean sortable silt ($\overline{SS}$) reflecting bottom-current speed; **(c)** XRF-derived sedimentary ln(Zr/Al) ratio, which is dependent on bottom-current speed (Bahr et al., 2014) and advection of fine-grained material from the nepheloid layer; and **(d)** CWC abundances based on CT scanning. Phases of CWC proliferation appear to require background state of high hydrodynamic conditions (elevated ln(Zr/Al) and $\overline{SS}$) but do not show an influence of deep-water-mass variability (δ^{13}C). Light red shadings denote intervals, with coral contents > 7 % used for discriminant analysis; blue arrows indicate erosive unconformities.

ample is the coral-free, high-TOC interval between 15 and 60 cm (Fig. 6). However, as suggested in the previous section, there are multiple factors necessary for stimulating coral growth at Bowie Mound.

To investigate the origin of the organic matter within the sediment matrix, we analyzed its C_{org} / N_{total} ratio and stable-carbon-isotopic composition ($\delta^{13}C_{org}$). Marine organic matter has lower C_{org} / N_{total} ratios (∼ 6.6) compared to terrestrial organic matter (> 20; Holtvoeth et al., 2003). Organic matter in core M125-34-2 exhibits C_{org} / N_{total} ratios of 14 to 52 (Fig. 6), indicating that land-derived material was a dominant source of organic matter throughout the record. Intervals of high CWC abundances are characterized by elevated C_{org} / N_{total} ratios, namely at the top and at the base of the core, with ratios of > 40, indicating an overwhelming contribution of terrigenous matter. Notably, in line with the upwelling center off Cabo Frio being confined to the shelf without reaching northward to the slope, where Bowie Mound is situated (Albuquerque et al., 2014, 2016), upwelling-derived organic matter with typical marine C_{org} / N_{total} ratios below 6.5 (Albuquerque et al., 2014) apparently played a subordinate role. A significant terrigenous admixture of terrestrial organic matter is also indicated by the relatively low $\delta^{13}C_{org}$ (−23.2 to −20.2 ‰) as terrigenous organic material has a more depleted signature (−27 ‰) compared to typical marine-$\delta^{13}C_{org}$ values (−19 ‰; Holtvoeth et al., 2003). In this regard, high $\delta^{13}C_{org}$ values during CWC-bearing intervals in the upper 50 cm and below 549.5 cm can be interpreted as periods of enhanced marine productivity, which contradicts contemporaneous C_{org} / N_{total} ratios of as high as 52. This conflicting evidence might be resolved by interpreting the high $\delta^{13}C_{org}$ values as being influenced by enhanced input of POC from C4 plants (typically grasses), which are characterized by an end-member of ca. −12 ‰ (Holtvoeth et al., 2003). Palynological evidence indeed points to the establishment of grassland biomes in the catchment of the Paraíba do Sul during the last glacial as a result of generally drier conditions (Behling et al., 2002). This is in accordance with the presumed deposition of the inter-

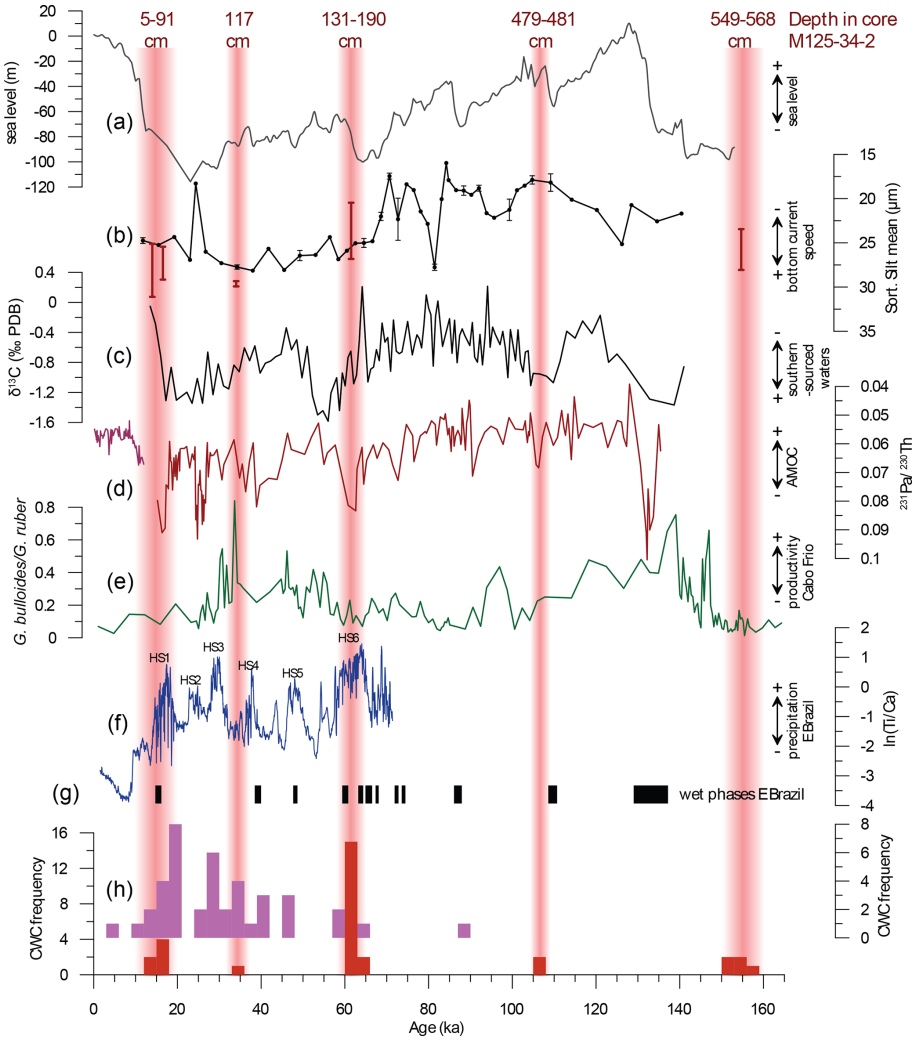

Figure 5. Frequency of CWC occurrences in the time domain at Bowie Mound core M125-34-2 and adjacent cores from the southeastern Brazilian margin in the paleoclimatic context. **(a)** Global sea level (Grant et al., 2012); **(b)** mean sortable silt in off-mound core M125-50-3 – range of sortable-silt values of CWC-bearing intervals in core M125-34-2 are indicated by red bars; **(c)** benthic δ^{13}C of *Uvigerina* spp. in off-mound core M125-50-3, reflecting the portion of southern-sourced waters (AAIW) at the southeastern Brazilian margin; **(d)** variability of Atlantic Meridional Overturning Circulation (AMOC; dark red line: Böhm et al., 2015; purple: Lippold et al., 2019); **(e)** upwelling intensity at Cabo Frio, reflected by the ratio between upwelling-related planktonic foraminifer *Globigerinoides bulloides* and oligotrophic *Globigerinoides ruber*; **(f)** ln(Ti/Ca) ratio, reflecting terrigenous input to the eastern Brazilian margin off the São Francisco River (core M125-95-3; Campos et al., 2019); **(g)** growth periods of travertine and speleothems in eastern Brazil during anomalous wet periods, indicated by black bars (Wang et al., 2004); **(h)** frequency of CWC Th/U dates per 3 kyr bins at Bowie Mound (core M125-34-2; red bars) and in cores at the southeastern Brazilian margin (violet; Mangini et al., 2010; Ruckelshausen, 2013; Fig. 1). Note the good match between CWC occurrences and enhanced monsoonal activity on the continent (correlation between ln(Ti/Ca) and CWC frequency: $r = 0.56$, $p = 0.02$; computed using the SurrogateCor function of the R package "astrochron"; Meyers, 2014). Red bars indicate periods of enhanced CWC growth at Bowie Mound, with the respective depths in core M125-34-2 annotated.

vals 0–50 cm and 549.5–568 cm during the last deglaciation and MIS 6, respectively (Fig. 5).

5.1.3 Influence of the continental hydrological cycle

A major source of terrigenous material and thus a potent organic-matter source for the Brazilian margin are rivers draining the densely vegetated hinterland, especially the Paraíba do Sul (Fig. 1). To investigate if enhanced riverine input due to more humid conditions in the hinterland increased terrestrial organic-matter supply to Bowie Mound, we studied the mineralogical and geochemical composition of the terrigenous fraction of the sediment. Changes in the water availability in the hinterland should impact the degree of weathering and thus leave an imprint in the mineralog-

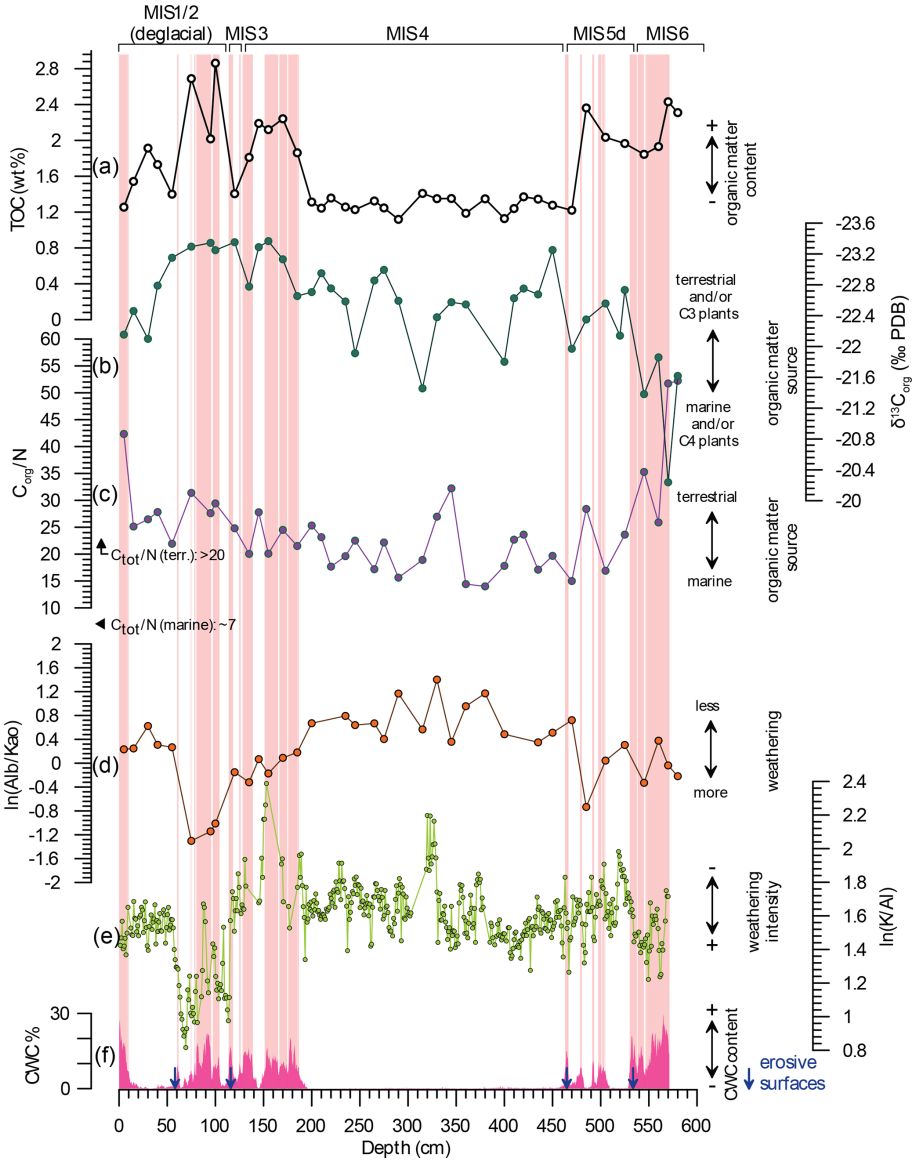

Figure 6. Organic-matter accumulation and origin at Bowie Mound core M125-34-2 in context with continental hydroclimate and CWC occurrences. **(a)** Total organic carbon (TOC; white dots), reflecting organic-matter accumulation; **(b)** and **(c)** show $\delta^{13}C$ and C_{org} / N_{tot} ratio of organic matter as measures for terrestrial vs. marine organic-matter input, respectively. Marine and terrestrial end-members are indicated (Holtvoeth et al., 2003). Panels **(d)** and **(e)** show XRD-derived ln(Albite / Kaolinite) and XRF-derived ln(K/Al) ratios, respectively, as indicators of the weathering intensity in the hinterland, reflecting the strength of the continental hydrological cycle, and **(f)** shows CWC abundances based on CT scanning. Note that high CWC abundances fall into intervals of high TOC and increased weathering due to an intensified continental hydrological cycle. Light-red shadings denote intervals with coral contents > 7 % used for discriminant analysis; blue arrows indicate erosive unconformities.

ical composition of the terrigenous sediments. The composition of the noncarbonaceous mineral phases is typical for soils that underwent different degrees of chemical weathering, comprising intermediate weathering products such as hydrobiotite (11.5 %, up to 24 %; Coleman et al., 1963; Wilson, 1970; Meunier and Velde, 1979) as well as typical constituents of soils that have been deeply weathered under tropical humid conditions such as kaolinite (7.9 % up to 15.3 %); gibbsite (on average 21.7 %); and Ca-, K-, and Al-rich zeolite (6.7 %; e.g., Weaver, 1975; Hughes, 1980; Ibrahim and Hall, 1996; Furian et al., 2002; cf. Appendix Table A). When comparing minerals typical for residual soils such as kaolinite, gibbsite, and zeolite with feldspar and mica, both groups are anticorrelated (Table 1) and exhibit distinct fluctuations throughout the core (the albite vs. kaolinite ratio is depicted in Fig. 6). Relatively high abundances of weathering residu-

Table 1. Correlation between terrigenous-mineral phases in core M125-34-2. Positive correlations are marked by bold font (for $r > 0.4$), negative correlations (for $r < 0.4$) in italics.

	Quartz	Gibbsite	Kaolinite	Muscovite	Hydrobiotite	Microcline	Zeolite
Quartz							
Gibbsite	−0.07						
Kaolinite	*−0.52*	−0.09					
Muscovite	0.35	**0.45**	−0.31				
Hydrobiotite	−0.34	*−0.62*	**0.55**	*−0.69*			
Microcline	**0.49**	−0.26	*−0.43*	−0.15	−0.02		
Zeolite	−0.16	0.68	0.00	**0.62**	*−0.43*	*−0.51*	
Albite	**0.65**	−0.07	*−0.76*	**0.47**	*−0.44*	0.35	−0.07

als like kaolinite are particularly present in the CWC-bearing interval between ca. 60 and 200 cm and to a lesser extent below 560 cm. This XRD-based data are also partly supported by the high-resolution ln(K/Al) record obtained via XRF scanning, which is particularly low during the interval 60–120 cm and below 530 cm (Fig. 6). Low ln(K/Al) ratios are consistent with high kaolinite contents, reflecting periods of strong K removal from soils due to chemical weathering during humid conditions in the hinterland. As the C_{org} / N_{total} ratio is also elevated during periods of low ln(K/Al) ratios and high kaolinite contents (Fig. 6), it can be inferred that high precipitation in the hinterland enhanced chemical weathering and increased terrigenous-organic-matter transport to the continental slope. Stronger chemical weathering would have also enhanced the input of Fe to the continental slope (Govin et al., 2012), leading to fertilization of the surface waters, which likely further invigorated surface productivity and increased the food supply for CWCs at Bowie Mound.

To objectively evaluate the relative importance of terrestrial organic-matter supply over changes in the hydraulic conditions in influencing CWC proliferation at Bowie Mound, we performed a discriminant analysis over $n = 34$ samples using (i) ln(Alb/Kao) as a weathering proxy, (ii) $\overline{SS}$ for bottom-current speed, and (iii) $\delta^{13}C_{org}$ and (iv) C_{org} / N_{total} for organic-matter provenance as predictors for the occurrences of CWC abundances above 7 % (reflecting representative CWC accumulations). Note that the $\delta^{13}C$ of benthic foraminifera has not been included due to the high scatter of the data. The restriction on those four parameters was also done to avoid unreliable results by overprediction. The outcome of the discriminant analysis yields a correct classification of 76 %, with highest skills in ln(Alb/Kao) (loading of −0.68) and C_{org} / N_{total} (+0.58), while loadings for $\overline{SS}$ (+ 0.06) and $\delta^{13}C_{org}$ (0.00) are insignificant (see Appendix Table B for details). This is consistent with peak CWC abundances during phases of strong hydrological activity, as evidenced by intensified chemical weathering (i.e., low ln(Alb/Kao) ratios), which enhanced the input of terrigenous organic matter (high C_{org} / N_{total}) to Bowie Mound and directly or indirectly (via surface water fertilization) stimulated CWC proliferation.

5.2 CWCs at Bowie Mound in the paleoclimatological context

As discussed above, phases of enhanced CWC proliferation at Bowie Mound occurred in parallel to periods of increased terrigenous POC and/or DOC input due to enhanced runoff. The most distinct CWC proliferation phases in fact took place during phases of anomalously strong monsoonal precipitation during the pronounced Heinrich stadials (HSs) 1 and 6 as well as (within age model uncertainties) during the shorter and less severe humid phases corresponding to HSs 2–5 (Fig. 5f, g). The prominent growth phase during HSs is in agreement with published CWC occurrences along the southeastern Brazilian margin from the same time frame (Mangini et al., 2010; Ruckelshausen, 2013; Figs. 1, 5g), indicating that our results are representative of a larger geographic area. The slow overturning circulation during HSs indicated by high $^{231}Pa/^{230}Th$ ratios (Fig. 5d; McManus et al., 2004; Böhm et al., 2015) resulted in enhanced precipitation over southeastern and eastern Brazil (Waelbroeck et al., 2018) due to heat accumulation in the Southern Hemisphere and intensification of the South Atlantic Convergence Zone (Fig. 1; Stríkis et al., 2015). Humid phases during HSs in otherwise dry eastern Brazil are documented by growth phases of speleothems and travertines (Fig. 5g), increased terrigenous input (core M125-95-3; Fig. 5f; Campos et al., 2019), and a slight expansion of forest cover (Gu et al., 2018). It is possible that the riverine suspension load from other rivers in eastern Brazil was advected southward by the BC and added to the enhanced terrigenous load from rivers adjacent to Bowie Mound (mostly the Paraíba do Sul). Due to the baffling capacity of framework-building CWCs (Mienis et al., 2007; Huvenne et al., 2009; Titschack et al., 2015), the additional sedimentary input would have aided mound formation. This nutrient- and organic-rich suspension potentially also enhanced marine surface productivity and thus directly and/or indirectly boosted food supply to the CWCs. As fresh-

water admixture to the SMW and SACW may have increased water column stratification and hence the density contrast to the AAIW, the concentration of sediment and food particles at the nepheloid layer may also have been more pronounced. The link between monsoonal activity and CWC growth proposed here is in line with studies from the western Mediterranean Sea (Fentimen et al., 2020), the Gulf of Cádiz (Wienberg et al., 2010), and the tropical eastern Atlantic off Angola (Hanz et al., 2019), which all inferred that terrestrial input via dust or fluvial runoff can ultimately fuel CWC colonies.

Notably, HSs occurred during phases of intermediate and low sea level, which facilitated the bypass of sediment across the shelf and thus allowed for an efficient supply of terrestrial organic matter to Bowie Mound (Fig. 5a). As discussed in Raddatz et al. (2020), during glacials, when sea level was up to 120 m lower than present (Waelbroeck et al., 2002; Rohling et al., 2014), water-mass boundaries may have been forced to migrate downslope. Such a displacement of water-mass boundaries would have moved the SACW–AAIW interface and the corresponding nepheloid layer from its present position at $\sim$ 500 m closer to the depth of Bowie Mound ($\sim$ 860 m), aiding the concentration and dispersal of food along the slope towards the CWC colonies. This suspected influence of sea level on the bottom-current dynamics at the depth of Bowie Mound is in fact evident from a sortable-silt record obtained from the off-mound site M125-50-3, which shows high (low) current speeds during low (high) sea level (Fig. 5b).

Hence, we argue that a dynamic hydraulic regime along with a pronounced nepheloid layer was required for CWCs to flourish at Bowie Mound (Mienis et al., 2007). These prerequisite conditions were present throughout glacial periods, during which the development of widespread glacial unconformities and extensive drift bodies along the southeast Brazilian margin (Viana et al., 1998; Viana, 2001) is evidence for such intense bottom-current activity. This is notably different from the slope south of the Abrolhos Bank, where reference core M125-50-3 is situated. Here, contouritic sediments and distinct hiatuses are largely absent in water depths affected by the AAIW and SACW, which testifies to less dynamic hydrological conditions (Bahr et al., 2016), potentially responsible for the lack of CWC mounds at this location. At the same time, $\overline{\mathrm{SS}}$ and ln(Zr/Al) data from both Bowie Mound core M125-34-2 (Fig. 4b) and off-mound core M125-50-3 (Fig. 5B) indicate that bottom-current speed was not anomalously high during HSs relative to the glacial background level. Hence, the distinct, pulse-like CWC growth phases at Bowie Mound could have been initiated by enhanced nutrient and organic-matter supply from land, as evidenced by the high C_{org} / N ratio of the organic matter. Surface water fertilization by the increase in terrigenous organic matter may have also improved marine primary productivity and contributed to higher export production, further fueling CWC growth. As discussed before, marine productivity caused by upwelling on the shelf of Cabo Frio was apparently of minor importance. Based on planktic foraminiferal assemblages (Lessa et al., 2019), enhanced upwelling occurred between HSs 3 and 4 at around 35 ka, when a small peak of CWC abundances occurs (Fig. 5g). However, during all other instances of CWC occurrences, upwelling at Cabo Frio was relatively low and likely did not reach as far north as Bowie Mound (Albuquerque et al., 2014, 2016).

We hence infer that CWC proliferation at Bowie Mound occurred simultaneously with an enhanced delivery of terrestrial organic matter towards the continental slope under glacial boundary conditions of low sea level and enhanced hydrodynamic activity along the slope. This implies the direct utilization of terrestrial organic matter by the corals and thus clearly stresses the necessity for future in-depth studies of the food preferences of *S. variabilis*.

6 Conclusions

Here we present a comprehensive multiproxy study of a CWC-bearing core retrieved off southeastern Brazil with the aim of assessing the relative importance of different environmental factors that supported and/or prohibited CWC proliferation and coral mound formation. We find that intervals of high CWC abundance are primarily related to millennial-scale high-latitude cold events (Heinrich Stadials) that were characterized by major reconfigurations of deep-ocean circulation and enhanced monsoonal precipitation in eastern Brazil. The dominance of terrigenous- over marine-derived organic matter during phases of fast CWC proliferation indicates that strong runoff enhanced the input of nutrients and food to coral mounds on the continental slope. Intensified hydrodynamic conditions at the water depth of Bowie Mound during sea-level lowstands thereby provided the necessary background conditions for an efficient dispersal of nutrient and food supply towards the upper and mid slope. Thus, this study presents a prime example of the intimate coupling between continental hydroclimate and ecological changes in the deep ocean.

Appendix A

Table A1. Major noncarbonaceous mineral phases in core M125-34-2 derived from Rietveld analyses of X-ray diffractometry.

Depth (cm)	Quartz (%)	Gibbsite (%)	Kaolinite (%)	Muscovite (%)	Hydrobiotite (%)	Microcline (%)	Zeolite (%)	Albite (%)
5	8.5	20.2	5.7	5.6	7.8	7.0	6.7	7.2
15	8.0	19.1	7.8	5.5	16.1	4.6	6.7	10.0
30	6.9	18.7	6.5	2.1	10.1	6.3	4.2	12.1
40	7.6	20.3	7.7	3.4	17.1	9.3	3.8	10.5
55	10.4	18.4	8.7	4.0	14.1	3.7	5.0	11.3
75	4.6	20.0	15.3	4.8	20.2	2.1	6.5	4.2
95	4.3	17.6	12.0	4.4	21.7	4.8	5.9	3.8
100	4.8	16.4	12.6	5.6	24.0	3.2	6.2	4.6
120	9.7	15.5	10.3	4.4	18.2	6.2	4.7	8.9
135	8.3	24.5	9.9	9.4	12.9	4.3	6.7	7.2
145	7.1	24.1	9.0	5.1	17.4	3.3	7.1	9.6
155	7.8	25.9	10.2	11.5	7.8	4.6	7.9	8.6
170	7.6	22.3	9.0	6.1	17.6	4.0	7.1	9.8
185	9.2	25.1	7.4	11.5	6.0	6.2	7.4	8.9
200	10.2	21.3	6.2	6.2	12.5	7.9	6.6	12.2
235	9.2	20.6	5.4	13.3	10.7	3.6	7.4	12.0
245	9.5	22.6	6.5	13.2	5.7	5.8	6.8	12.4
265	8.1	22.8	6.5	9.9	9.8	6.4	7.4	12.7
275	9.2	23.5	7.5	12.9	6.9	5.4	7.0	11.3
290	9.6	21.6	4.0	10.7	9.7	6.9	6.3	13.0
315	10.4	21.9	6.3	12.8	7.1	5.0	6.7	11.1
330	9.3	19.8	4.0	11.4	8.7	5.1	6.4	16.3
345	7.7	19.7	8.3	11.9	10.2	4.9	7.1	11.9
360	6.9	19.4	5.5	9.0	10.0	5.8	6.3	14.3
380	8.3	23.1	4.5	13.7	5.2	3.2	7.2	14.5
400	7.0	21.2	6.2	7.6	12.9	6.8	6.5	10.1
435	7.9	23.1	8.3	12.6	6.2	3.1	6.8	11.8
450	7.8	23.1	7.0	12.0	7.4	3.8	7.4	11.7
470	8.3	18.6	6.4	11.8	14.6	4.6	7.5	13.2
485	6.3	27.4	12.2	12.3	5.5	2.8	8.5	5.8
505	5.5	23.7	9.5	12.5	6.2	2.8	7.7	9.9
525	5.7	24.6	7.4	10.2	11.2	3.6	8.0	10.1
545	4.4	23.1	8.4	4.4	10.3	3.0	7.4	6.0
560	6.5	26.3	5.3	6.8	8.1	3.8	7.1	7.8
570	5.8	22.0	7.3	6.0	10.5	3.5	6.4	7.0
580	5.3	23.0	8.1	5.8	12.9	2.8	7.3	6.5

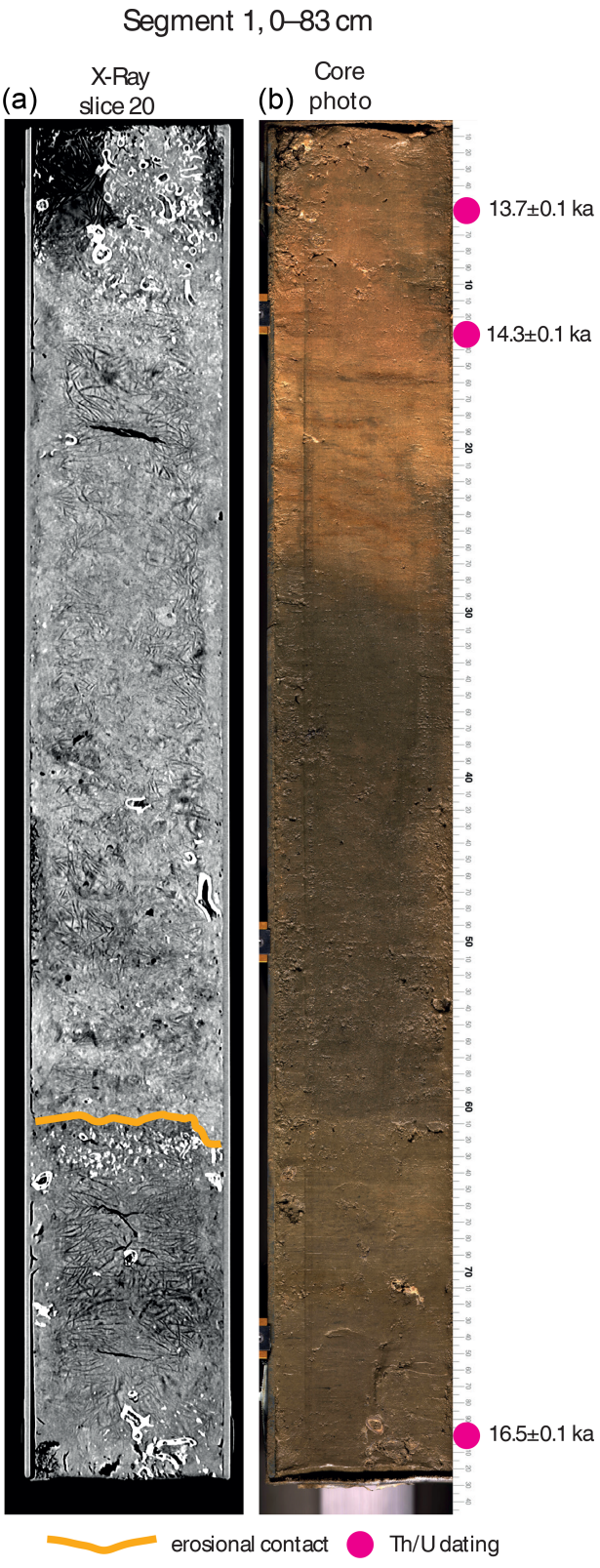

Figure A1. CT image **(a)** and photography **(b)** of segment 0–83 cm of core M125-34-2. Erosional contacts are marked by thick black lines; position of Th/U datings with calibrated ages are indicated by magenta dots.

Appendix B

Table B1. Result of discriminant analysis performed on detrended and normalized proxies obtained in core M125-34-2. Samples were divided into classes with CWC contents > 7 % (labeled "1") and < 7 % ("0"). Classes derived from discriminant analysis are displayed in the last column, with wrongly assigned classes marked in bold. PDB: Pee Dee Belemnite.

Depth (cm)	ln(Alb/Kao)	$\overline{SS}$ (µm)	$\delta^{13}C_{org}$ (‰ PDB)	C_{org} / N	CWC > 7%	Inferred class
5	0.01	0.71	0.58	2.03	1	1
15	0.03	−0.61	0.11	0.04	0	0
30	0.64	1.73	0.67	0.20	0	0
40	0.13	1.94	−0.39	0.35	0	0
55	0.06	0.84	−0.95	−0.33	0	0
75	−2.49	0.15	−1.17	0.77	1	1
95	−2.23	0.86	−1.24	0.33	1	1
100	−2.01	0.81	−1.10	0.54	1	1
120	−0.61	1.16	−1.25	0.00	0	**1**
135	−0.89	−1.07	−0.37	−0.55	1	**0**
145	−0.26	−1.61	−1.16	0.35	0	0
155	−0.65	−1.30	−1.28	−0.54	1	**0**
170	−0.22	0.54	−0.91	−0.03	1	**0**
185	−0.08	−0.85	−0.18	−0.38	1	**0**
200	0.72	0.53	−0.26	0.06	0	0
235	0.92	0.40	−0.08	−0.60	0	0
245	0.67	0.88	0.95	−0.26	0	0
265	0.72	0.04	−0.49	−0.88	0	0
275	0.29	1.00	−0.71	−0.30	0	0
290	1.53	1.17	−0.09	−1.06	0	0
315	0.55	0.40	1.65	−0.68	0	0
330	1.91	−0.27	0.24	0.25	0	0
345	0.21	−0.72	−0.06	0.86	0	0
400	0.42	0.12	1.12	−0.80	0	0
435	0.20	−0.87	−0.22	−0.88	0	0
450	0.46	0.41	−1.10	−0.59	0	0
470	0.80	−1.26	0.86	−1.13	0	0
485	−1.56	−1.98	0.28	0.42	0	**1**
505	−0.30	−2.22	−0.04	−0.91	0	0
525	0.13	−2.01	−0.30	−0.13	0	0
545	−0.90	−1.44	1.77	1.21	0	**1**
560	0.24	0.11	1.03	0.13	1	**0**
570	−0.43	−0.85	3.52	3.12	1	1
580	−0.72	0.82	1.40	3.17	1	1

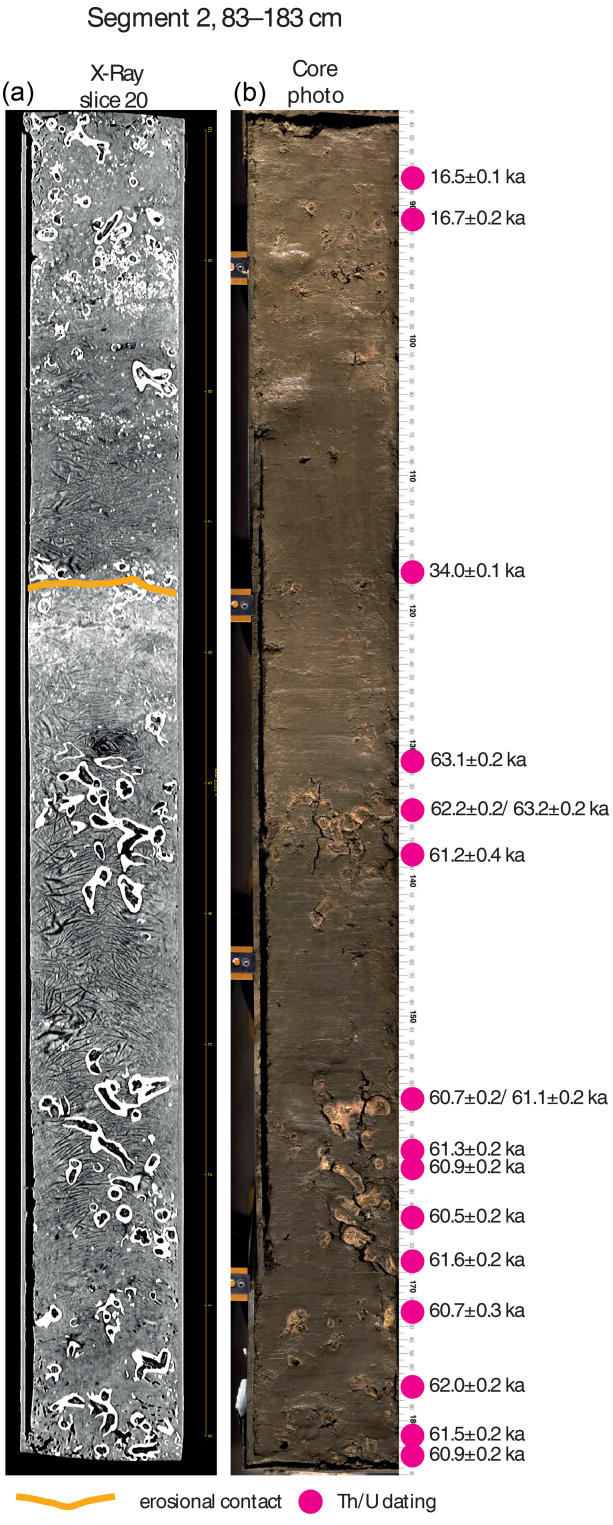

Figure B1. CT image **(a)** and photography **(b)** of segment 83–183 cm of core M125-34-2. Erosional contacts are marked by thick black lines; position of Th/U datings with calibrated ages are indicated by magenta dots.

Appendix C

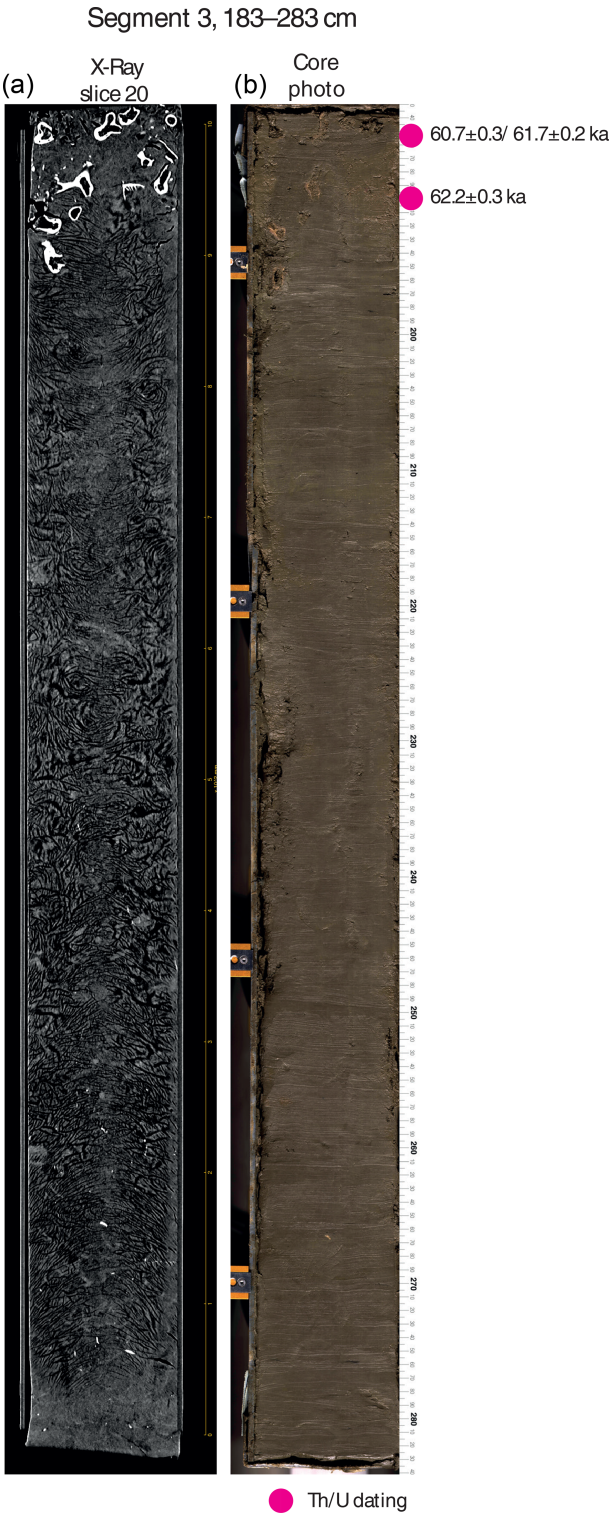

Figure C1. CT image **(a)** and photography **(b)** of segment 183–283 cm of core M125-34-2. Position of Th/U dating with calibrated age is indicated by a magenta dot.

Appendix D

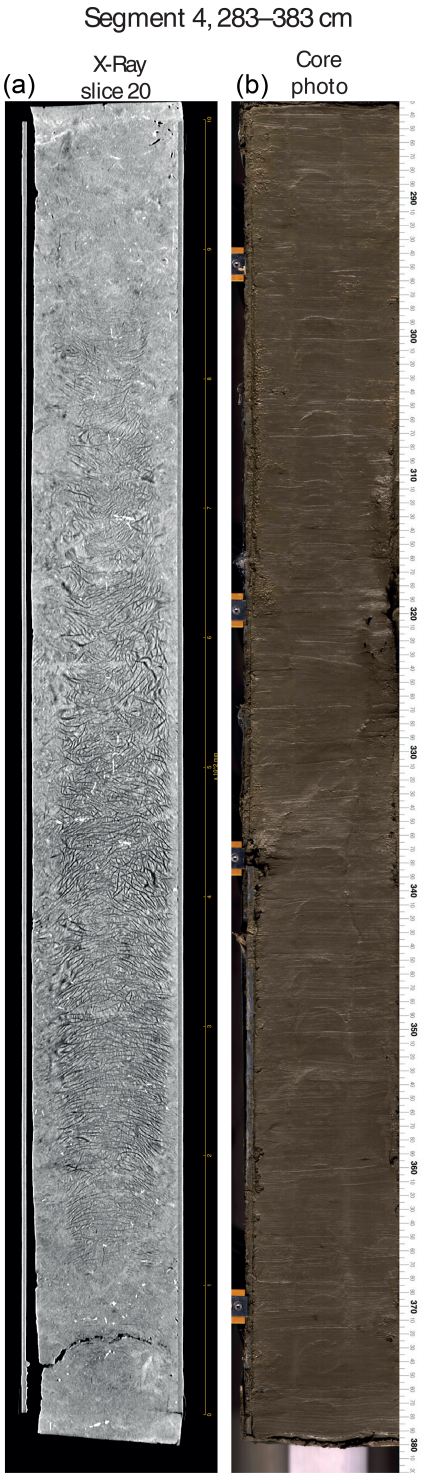

Figure D1. CT image **(a)** and photography **(b)** of segment 283–383 cm of core M125-34-2.

Appendix E

Figure E1. CT image **(a)** and photography **(b)** of segment 383–483 cm of core M125-34-2. Erosional contacts are marked by thick black lines; position of Th/U dating with calibrated age is indicated by a magenta dot.

Appendix F

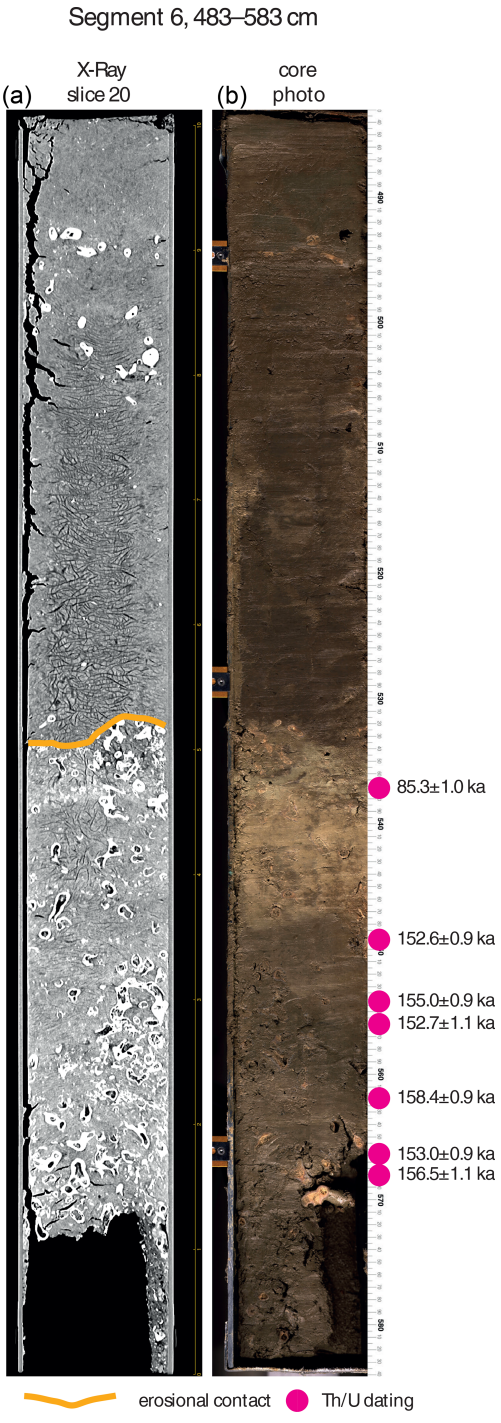

Figure F1. CT image **(a)** and photography **(b)** of segment 383–483 cm of core M125-34-2. Erosional contacts are marked by thick black lines; positions of Th/U datings with calibrated age are indicated by magenta dots.

Data availability. All data presented in this study will be made available in the Pangaea database (https://www.pangaea.de/, last access: 16 November 2020, Diepenbroek et al., 2002).

Author contributions. AB and JR designed the study. AB, MD, JT, GA, DN, AK, and JR were involved in sampling and data generation. All authors contributed to data interpretation and manuscript writing.

Competing interests. The authors declare that they have no conflict of interest.

Acknowledgements. We thank the captain and crew of R/W *METEOR* for their support during expedition M125. We further kindly acknowledge Ilse Glass (X-ray diffractometry); Doris Bergmann-Dörr (carbon and nitrogen analysis); Swaantje Brzelinski, Carolina Catunda, Sebastian Fessler, Jens Fiebig, Sven Hofmann, and Bernd Knape (stable-oxygen- and stable-carbon-isotope analysis); Nadine Gehre (sample preparation and foraminiferal selection); and Larissa Frede (sortable-silt analysis) for support during sample preparation and analyses. The authors are grateful to Wolfram Stiller and Stephan Skornitzke from the Heidelberg University Hospital for performing the CT scanning.

Financial support. This research has been supported by the Deutsche Forschungsgemeinschaft (grant nos. HO5927/1-1 to André Bahr and EXC-2077 – 390741603 to Jürgen Titschack).

Review statement. This paper was edited by Aninda Mazumdar and reviewed by Robin Fentimen and one anonymous referee.

References

Addamo, A. M., Vertino, A., Stolarski, J., García-Jiménez, R., Taviani, M., and Machordom, A.: Merging scleractinian genera: the overwhelming genetic similarity between solitary *Desmophyllum* and colonial *Lophelia*, BMC Evol. Biol., 16, 108, https://doi.org/10.1186/s12862-016-0654-8, 2016.

Aguiar, A. L., Cirano, M., Pereira, J., and Marta-Almeida, M.: Upwelling processes along a western boundary current in the Abrolhos–Campos region of Brazil, Cont. Shelf Res., 85, 42–59, https://doi.org/10.1016/j.csr.2014.04.013, 2014.

Albuquerque, A. L., Meyers, P., Belem, A. L., Turcq, B., Siffedine, A., Mendoza, U., and Capilla, R.: Mineral and elemental indicators of post-glacial changes in sediment delivery and deposition under a western boundary upwelling system (Cabo Frio, southeastern Brazil), Palaeogeogr. Palaeocl., 445, 72–82, https://doi.org/10.1016/j.palaeo.2016.01.006, 2016.

Albuquerque, A. L. S., Belem, A. L., Zuluaga, F. J., Cordeiro, L. G., Mendoza, U., Knoppers, B. A., Gurgel, M. H., Meyers, P. A., and Capilla, R.: Particle fluxes and bulk geochemical characterization of the Cabo Frio upwelling system in Southeastern Brazil: Sediment trap experiments between Spring 2010 and Summer 2012, An. Acad. Bras. Cienc., 86, 601–620, 2014.

Auscavitch, S. R., Deere, M. C., Keller, A. G., Rotjan, R. D., Shank, T. M., Cordes, E. E.: Oceanographic drivers of deep-sea coral species distribution and community assembly on seamounts, islands, atolls, and reefs within the Phoenix Islands Protected Area, Front. Mar. Sci., 7, 42, doi:10.3389/fmars.2020.00042, 2020.

Bahr, A., Jiménez-Espejo, F. J., Kolasinac, N., Grunert, P., Hernández-Molina, F. J., Röhl, U., Voelker, A. H., Escutia, C., Stow, D. A., and Hodell, D.: Deciphering bottom current velocity and paleoclimate signals from contourite deposits in the Gulf of Cádiz during the last 140 kyr: An inorganic geochemical approach, Geochem. Geophys. Geosys., 15, 3145–3160, doi:10.1002/ggge.20106, 2014.

Bahr, A., Spadano Albuquerque, A., Ardenghi, N., Batenburg, S., Bayer, M., Catunda, M., Conforti, A., Dias, B., Dias Ramos, R., and Egger, L.: South American Hydrological Balance and Paleoceanography during the Late Pleistocene and Holocene (SAMBA)–Cruise No. M125, March 21–April 15, 2016-Rio de Janeiro (Brazil)–Fortaleza (Brazil), DFG-Senatskommission für Ozeanographie, Bremen, 2016.

Behling, H., Arz, H. W., Pätzold, J., and Wefer, G.: Late Quaternary vegetational and climate dynamics in southeastern Brazil, inferences from marine cores GeoB 3229-2 and GeoB 3202-1, Palaeogeogr. Palaeocl., 179, 227–243, 2002.

Bianchi, G. G., Vautravers, M. J., and Shackleton, N. J.: Deep flow variability under apparently stable North Atlantic Deep Water production during the last interglacial of the subtropical NW Atlantic, Paleoceanography, 16, 306–316, 2001.

Böhm, E., Lippold, J., Gutjahr, M., Frank, M., Blaser, P., Antz, B., Fohlmeister, J., Frank, N., Andersen, M. B., and Deininger, M.: Strong and deep Atlantic meridional overturning circulation during the last glacial cycle, Nature, 517, 73–76, doi:10.1038/nature14059, 2015.

Bostock, H. C., Tracey, D. M., Currie, K. I., Dunbar, G. B., Handler, M. R., Fletcher, S. E. M., Smith, A. M., and Williams, M. J.: The carbonate mineralogy and distribution of habitat-forming deep-sea corals in the southwest pacific region, Deep Sea Res. Pt. I, 100, 88–104, 2015.

Büscher, J. V., Form, A. U., and Riebesell, U.: Interactive effects of ocean acidification and warming on growth, fitness and survival of the cold-water coral *Lophelia pertusa* under different food availabilities, Front. Mar. Sci., 4, 101, https://doi.org/10.3389/fmars.2017.00101, 2017.

Campos, M. C., Chiessi, C. M., Prange, M., Mulitza, S., Kuhnert, H., Paul, A., Venancio, I. M., Albuquerque, A. L. S., Cruz, F. W., and Bahr, A.: A new mechanism for millennial scale positive precipitation anomalies over tropical South America, Quaternary Sci. Rev., 225, 105990, https://doi.org/10.1016/j.quascirev.2019.105990, 2019.

Carvalho, C., Salomão, M., Molisani, M., Rezende, C., and Lacerda, L.: Contribution of a medium-sized tropical river to the particulate heavy-metal load for the South Atlantic Ocean, Sci. Total Environ., 284, 85–93, 2002.

Carvalho, L. M., Jones, C., and Liebmann, B.: The South Atlantic convergence zone: Intensity, form, persistence, and relationships with intraseasonal to interannual activity and extreme rainfall, J. Clim., 17, 88–108, 2004.

Castelao, R. M. and Barth, J. A.: The relative importance of wind strength and along-shelf bathymetric variations on the separation of a coastal upwelling jet, J. Phys. Oceanogr., 36, 412–425, 2006.

Castelao, R. M.: Sea surface temperature and wind stress curl variability near a cape, J. Phys. Oceanogr., 42, 2073–2087, 2012.

Cathalot, C., Van Oevelen, D., Cox, T. J., Kutti, T., Lavaleye, M., Duineveld, G., and Meysman, F. J.: Cold-water coral reefs and adjacent sponge grounds: Hotspots of benthic respiration and organic carbon cycling in the deep sea, Front. Mar. Sci., 2, 37, https://doi.org/10.3389/fmars.2015.00037, 2015.

Coleman, N., LeRoux, F., and Cady, J. G.: Biotite-hydrobiotite-vermiculite in soils, Nature, 198, 409–410, 1963.

Curry, W. B. and Oppo, D. W.: Glacial water mass geometry and the distribution of $\delta^{13}C$ of ΣCO_2 in the western Atlantic Ocean, Paleoceanography, 20, PA1017, https://doi.org/10.1029/2004PA001021, 2005.

Davies, A. J., Duineveld, G. C., Lavaleye, M. S., Bergman, M. J., van Haren, H., and Roberts, J. M.: Downwelling and deep-water bottom currents as food supply mechanisms to the cold-water coral*Lophelia pertusa* (Scleractinia) at the Mingulay Reef Complex, Limnol. Oceanogr., 54, 620–629, 2009.

Diepenbroek, M., Grobe, H., Reinke, M., Schindler, U., Schlitzer, R., Sieger, R., and Wefer, G.: PANGAEA – an information system for environmental sciences, available at: https://www.pangaea.de/ (last access: 16 November 2020), Comput. Geosci., 28, 1201–1210, 2002.

Dorschel, B., Hebbeln, D., Foubert, A., White, M., and Wheeler, A.: Hydrodynamics and cold-water coral facies distribution related to recent sedimentary processes at Galway Mound west of Ireland, Mar. Geol., 244, 184–195, 2007.

Duineveld, G. C., Lavaleye, M. S., Bergman, M. J., De Stigter, H., and Mienis, F.: Trophic structure of a cold-water coral mound community (Rockall Bank, NE Atlantic) in relation to the near-bottom particle supply and current regime, Bull. Mar. Sci., 81, 449–467, 2007.

Dullo, W.-C., Flögel, S., and Rüggeberg, A.: Cold-water coral growth in relation to the hydrography of the Celtic and Nordic European continental margin, Mar. Ecol. Prog. Ser., 371, 165–176, 2008.

Fallon, S., Thresher, R., and Adkins, J.: Age and growth of the cold-water scleractinian *Solenosmilia variabilis* and its reef on SW Pacific seamounts, Coral Reefs, 33, 31–38, 2014.

Fentimen, R., Feenstra, E., Rüggeberg, A., Vennemann, T., Hajdas, I., Adatte, van Rooij, D., and Foubert, A.: Cold-water coral mound archive provides unique insights into intermediate water mass dynamics in the Alboran Sea during the Last Deglaciation, Front. Mar. Sci., 7, 354, https://doi.org/10.3389/fmars.2020.00354, 2020.

Flögel, S., Dullo, W.-C., Pfannkuche, O., Kiriakoulakis, K., and Rüggeberg, A.: Geochemical and physical constraints for the occurrence of living cold-water corals, Deep Sea Res. Pt. II, 99, 19–26, 2014.

Form, A. U. and Riebesell, U.: Acclimation to ocean acidification during long-term CO_2 exposure in the cold-water coral *Lophelia pertusa*, Global Change Biol., 18, 843–853, 2012.

Frank, N., Freiwald, A., Correa, M. L., Wienberg, C., Eisele, M., Hebbeln, D., Van Rooij, D., Henriet, J.-P., Colin, C., and van Weering, T.: Northeastern Atlantic cold-water coral reefs and climate, Geology, 39, 743–746, 2011.

Frederiksen, R., Jensen, A., and Westerberg, H.: The distribution of the scleractinian coral *Lophelia pertusa* around the Faroe Islands and the relation to internal tidal mixing, Sarsia, 77, 157–171, 1992.

Furian, S., Barbiero, L., Boulet, R., Curmi, P., Grimaldi, M., and Grimaldi, C.: Distribution and dynamics of gibbsite and kaolinite in an oxisol of Serra do Mar, southeastern Brazil, Geoderma, 106, 83–100, 2002.

Gammon, M. J., Tracey, D. M., Marriott, P. M., Cummings, V. J., and Davy, S. K.: The physiological response of the deep-sea coral *Solenosmilia variabilis* to ocean acidification, Peerj, 6, e5236, https://doi.org/10.7717/peerj.5236, 2018.

Gori, A., Grover, R., Orejas, C., Sikorski, S., and Ferrier-Pagès, C.: Uptake of dissolved free amino acids by four cold-water coral species from the Mediterranean Sea, Deep Sea Res. Pt. II, 99, 42–50, 2014.

Govin, A., Holzwarth, U., Heslop, D., Ford Keeling, L., Zabel, M., Mulitza, S., Collins, J. A., and Chiessi, C. M.: Distribution of major elements in Atlantic surface sediments (36° N–49° S): Imprint of terrigenous input and continental weathering, Geochem. Geophys. Geosys., 13, Q01013, https://doi.org/10.1029/2011GC003785, 2012.

Grant, K. M., Rohling, E. J., Bar-Matthews, M., Ayalon, A., Medina-Elizalde, M., Ramsey, C. B., Satow, C., and Roberts, A. P.: Rapid coupling between ice volume and polar temperature over the past 150,000 years, Nature, 491, 744–747, doi:10.1038/nature11593, 2012.

Gu, F., Chiessi, C. M., Zonneveld, K. A. F., and Behling, H.: Late Quaternary environmental dynamics inferred from marine sediment core GeoB6211-2 off southern Brazil, Palaeogeogr. Palaeocl., 496, 48–61, https://doi.org/10.1016/j.palaeo.2018.01.015, 2018.

Hammer, Ø., Harper, D. A. T., and Ryan, P. D.: PAST: Paleontological statistics software package for education and data analysis, Palaeo. Electronica, 1, 4, 2001.

Hebbeln, D., Wienberg, C., Wintersteller, P., Freiwald, A., Becker, M., Beuck, L., Dullo, C., Eberli, G. P., Glogowski, S., Matos, L., Forster, N., Reyes-Bonilla, H., and Taviani, M.: Environmental forcing of the Campeche cold-water coral province, southern Gulf of Mexico, Biogeosciences, 11, 1799–1815, https://doi.org/10.5194/bg-11-1799-2014, 2014.

Hebbeln, D., da Costa Portilho-Ramos, R., Wienberg, C. and Titschack, J.: The fate of cold-water corals in a changing world: a geological perspective, Front. Mar. Sci., 119, https://doi.org/10.3389/fmars.2019.00119, 2019.

Hennige, S., Wicks, L., Kamenos, N., Perna, G., Findlay, H., and Roberts, J.: Hidden impacts of ocean acidification to live and dead coral framework, P. Roy. Soc. B-Biol. Sci., 282, https://doi.org/10.1098/rspb.2015.099020150990, 2015.

Hanz, U., Wienberg, C., Hebbeln, D., Duineveld, G., Lavaleye, M., Juva, K., Dullo, W.-C., Freiwald, A., Tamborrino, L., Reichart, G.-J., Flögel, S., and Mienis, F.: Environmental factors influencing benthic communities in the oxygen minimum zones on the Angolan and Namibian margins, Biogeosciences, 16, 4337–4356, https://doi.org/10.5194/bg-16-4337-2019, 2019.

Hernández-Molina, F. J., Stow, D. A. V., Alvarez-Zarikian, C. A., Acton, G., Bahr, A., Balestra, B., Ducassou, E., Flood, R., Flores, J.-A., Furota, S., Grunert, P., Hodell, D., Jimenez-Espejo, F., Kim, J. K., Krissek, L., Kuroda, J., Li, B., Llave,

E., Lofi, J., Lourens, L., Miller, M., Nanayama, F., Nishida, N., Richter, C., Roque, C., Pereira, H., Sanchez Goñi, M. F., Sierro, F. J., Singh, A. D., Sloss, C., Takashimizu, Y., Tzanova, A., Voelker, A., Williams, T., and Xuan, C.: Onset of Mediterranean outflow into the North Atlantic, Science, 344, 1244–1250, doi:10.1126/science.1251306, 2014.

Holtvoeth, J., Wagner, T., and Schubert, C. J.: Organic matter in river-influenced continental margin sediments: The land-ocean and climate linkage at the Late Quaternary Congo fan (ODP Site 1075), Geochem. Geophys. Geosys., 4, 1109, doi:1110.1029/2003GC000590, 2003.

Hughes, J.: Crystallinity of kaolin minerals and their weathering sequence in some soils from Nigeria, Brazil and Colombia, Geoderma, 24, 317–325, 1980.

Huvenne, V. A. I., Masson D. G., and Wheeler, A. J.: Sediment dynamics of a sandy contourite: The sedimentary context of the Darwin cold-water coral mounds, Northern Rockall Trough, Intern. J. Earth Sci., 98, 865–884, 2009.

Ibrahim, K. and Hall, A.: The authigenic zeolites of the Aritayn Volcaniclastic Formation, north-east Jordan, Miner. Deposita, 31, 514–522, doi:10.1007/BF00196131, 1996.

Jennerjahn, T., Knoppers, B., Souza, W., Carvalho, C., Mollenhauer, G., Hübner, M., and Ittekkot, V.: The tropical Brazilian continental margin, Carbon and Nutrient Fluxes in Continental Margins, a Global Synthesis, Berlin, Springer Verlag, Heidelberg, 427–436, 2010.

Jonkers, L., Prins, M. A., Brummer, G. J., Konert, M., and Lougheed, B. C.: Experimental insights into laser diffraction particle sizing of fine-grained sediments for use in palaeoceanography, Sedimentology, 56, 2192–2206, 2009.

Kaboth, S., Boer, B., Bahr, A., Zeeden, C., and Lourens, L. J.: Mediterranean Outflow Water dynamics during the past $\sim$570 kyr: Regional and global implications, Paleoceanography, 32, 634–647, 2017.

Kano, A., Ferdelman, T. G., Williams, T., Henriet, J.-P., Ishikawa, T., Kawagoe, N., Takashima, C., Kakizaki, Y., Abe, K., and Sakai, S.: Age constraints on the origin and growth history of a deep-water coral mound in the northeast Atlantic drilled during Integrated Ocean Drilling Program Expedition 307, Geology, 35, 1051–1054, 2007.

Kiriakoulakis, K., Fisher, E., Wolff, G. A., Freiwald, A., Grehan, A., and Roberts, J. M.: Lipids and nitrogen isotopes of two deep-water corals from the North-East Atlantic: initial results and implications for their nutrition, in: Cold-water Corals and Ecosystems, edited by: Freiwald, A. and Roberts, J. M., Springer, Erlangen, 715–729, 2005.

Kroopnick, P.: The distribution of ^{13}C of ΣCO_2 in the world oceans, Deep Sea Res. Pt. A., 32, 57–84, 1985.

Lessa, D. V., Santos, T. P., Venancio, I. M., Santarosa, A. C. A., dos Santos Jr., E. C., Toledo, F. A., Costa, K. B., and Albuquerque, A. L. S.: Eccentricity-induced expansions of Brazilian coastal upwelling zones, Global Planet. Change, 179, 33–42, 2019.

Lindberg, B. and Mienert, J.: Postglacial carbonate production by cold-water corals on the Norwegian shelf and their role in the global carbonate budget, Geology, 33, 537–540, 2005.

Lippold, J., Pöppelmeier, F., Süfke, F., Gutjahr, M., Goepfert, T. J., Blaser, P., Friedrich, O., Link, J. M., Wacker, L., Rheinberger, S., and Jaccard, S. L.: Constraining the variability of the Atlantic Meridional Overturning Circulation during the Holocene, Geophys. Res. Lett., 46, 11338–11346, doi:10.1029/2019gl084988, 2019.

Lisiecki, L. E. and Raymo, M. E.: A Pliocene-Pleistocene stack of 57 globally distributed benthic delta O-18 records, Paleoceanography, 20, PA1003, https://doi.org/10.1029/2004PA001071, 2005.

Lunden, J. J., McNicholl, C. G., Sears, C. R., Morrison, C. L., and Cordes, E. E.: Acute survivorship of the deep-sea coral Lophelia pertusa from the Gulf of Mexico under acidification, warming, and deoxygenation, Front. Mar. Sci., 1, 78, https://doi.org/10.3389/fmars.2014.00078, 2014.

Magill, C. R., Ausín, B., Wenk, P., McIntyre, C., Skinner, L., Martínez-García, A., Hodell, D. A., Haug, G. H., Kenney, W., and Eglinton, T. I.: Transient hydrodynamic effects influence organic carbon signatures in marine sediments, Nat. Commun., 9, 4690, https://doi.org/10.1038/s41467-018-06973-w, 2018.

Maier, C., Watremez, P., Taviani, M., Weinbauer, M., and Gattuso, J.: Calcification rates and the effect of ocean acidification on Mediterranean cold-water corals, P. Roy. Soc. B-Biol. Sci., 279, 1716–1723, 2012.

Mangini, A., Godoy, J., Godoy, M., Kowsmann, R., Santos, G., Ruckelshausen, M., Schroeder-Ritzrau, A., and Wacker, L.: Deep sea corals off Brazil verify a poorly ventilated Southern Pacific Ocean during H2, H1 and the Younger Dryas, Earth Planet. Sci. Lett., 293, 269–276, 2010.

Marchitto, T., Curry, W., Lynch-Stieglitz, J., Bryan, S., Cobb, K., and Lund, D.: Improved oxygen isotope temperature calibrations for cosmopolitan benthic foraminifera, Geochim. Cosmochim. Ac., 130, 1–11, 2014.

Marengo, J., Liebmann, B., Grimm, A., Misra, V., Silva Dias, P., Cavalcanti, I., Carvalho, L., Berbery, E., Ambrizzi, T., and Vera, C.: Recent developments on the South American monsoon system, Int. J. Climatol., 32, 1–21, 2012.

McCave, I. N., Manighetti, B., and Robinson, S. G.: Sortable silt and fine sediment size/composition slicing: parameters for palaeocurrent speed and palaeoceanography, Paleoceanography, 10, 593–610, 1995.

McManus, J. F., Francois, R., Gherardi, J.-M., Keigwin, L. D., and Brown-Leger, S.: Collapse and rapid resumption of Atlantic meridional circulation linked to deglacial climate changes, Nature, 428, 834–837, doi:10.1038/nature02494, 2004.

Mémery, L., Arhan, M., Álvarez-Salgado, X. A., Messias, M.-J., Mercier, H., Castro, C. G., and Ríos, A. F.: The water masses along the western boundary of the south and equatorial Atlantic, Prog. Oceanogr., 47, 69–98, 2000.

Meunier, A. and Velde, B.: Biotite Weathering in Granites of Western France, in: Developments in Sedimentology, edited by: Mortland, M. M. and Farmer, V. C., Elsevier, Amsterdam, Oxford, New York, 405–413, 1979.

Meyers, S.: Astrochron: An R package for astrochronology, available at: https://CRAN.R-project.org/package=astrochron (last access: 16 November 2020), 2014.

Mienis, F., De Stigter, H., White, M., Duineveld, G., De Haas, H., and Van Weering, T.: Hydrodynamic controls on cold-water coral growth and carbonate-mound development at the SW and SE Rockall Trough Margin, NE Atlantic Ocean, Deep Sea Res. Pt. I, 54, 1655–1674, 2007.

Mienis, F., Bouma, T., Witbaard, R., Van Oevelen, D., and Duineveld, G.: Experimental assessment of the effects of coldwater

coral patches on water flow, Mar. Ecol. Prog. Ser., 609, 101–117, 2019.

Miramontes, E., Penven, P., Fierens, R., Droz, L., Toucanne, S., Jorry, S. J., Jouet, G., Pastor, L., Silva Jacinto, R., Gaillot, A., Giraudeau, J., and Raisson, F.: The influence of bottom currents on the Zambezi Valley morphology (Mozambique Channel, SW Indian Ocean): In situ current observations and hydrodynamic modelling, Mar. Geol., 410, 42–55, https://doi.org/10.1016/j.margeo.2019.01.002, 2019.

Mueller, C. E., Larsson, A. I., Veuger, B., Middelburg, J. J., and van Oevelen, D.: Opportunistic feeding on various organic food sources by the cold-water coral Lophelia pertusa, Biogeosciences, 11, 123–133, https://doi.org/10.5194/bg-11-123-2014, 2014.

Muñoz, A., Cristobo, J., Rios, P., Druet, M., Polonio, V., Uchupi, E., Acosta, J., and Group, A.: Sediment drifts and cold-water coral reefs in the Patagonian upper and middle continental slope, Mar. Petrol. Geol., 36, 70–82, 2012.

Pahnke, K. and Zahn, R.: Southern hemisphere water mass conversion linked with North Atlantic climate variability, Science, 307, 1741–1746, 2005.

Pahnke, K., Goldstein, S. L., and Hemming, S. R.: Abrupt changes in Antarctic Intermediate Water circulation over the past 25,000 years, Nat. Geosci., 1, 870–874, 2008.

Poggemann, D.-W., Hathorne, E. C., Nürnberg, D., Frank, M., Bruhn, I., Reißig, S., and Bahr, A.: Rapid deglacial injection of nutrients into the tropical Atlantic via Antarctic Intermediate Water, Earth Planet. Sci. Lett., 463, 118–126, 2017.

Raddatz, J. and Rüggeberg, A.: Constraining past environmental changes of cold-water coral mounds with geochemical proxies in corals and foraminifera, The Depositional Record, 1–23, https://doi.org/10.1002/dep2.98, 2019.

Raddatz, J., Rüggeberg, A., Margreth, S., Dullo, W.-C., and Expedition, I.: Paleoenvironmental reconstruction of Challenger Mound initiation in the Porcupine Seabight, NE Atlantic, Mar. Geol., 282, 79–90, 2011.

Raddatz, J., Rüggeberg, A., Liebetrau, V., Foubert, A., Hathorne, E. C., Fietzke, J., Eisenhauer, A., and Dullo, W.-C.: Environmental boundary conditions of cold-water coral mound growth over the last 3 million years in the Porcupine Seabight, Northeast Atlantic, Deep Sea Res. Pt. II, 99, 227–236, 2014.

Raddatz, J., Liebetrau, V., Trotter, J., Rüggeberg, A., Flögel, S., Dullo, W. C., Eisenhauer, A., Voigt, S., and McCulloch, M.: Environmental constraints on Holocene cold-water coral reef growth off Norway: Insights from a multiproxy approach, Paleoceanography, 31, 1350–1367, 2016.

Raddatz, J., Titschack, J., Frank, N., Freiwald, A., Conforti, A., Osborne, A., Skornitzke, S., Stiller, W., Rüggeberg, A., Voigt, S., Albuquerque, A., Vertino, A., Schröder-Ritzrau, A., and Bahr, A.: *Solenosmilia variabilis*-bearing cold-water mounds off Brazil, Coral Reefs, 39, 69–83, doi:10.1007/s00338-019-01882-w, 2020.

Rathburn, A. E., Corliss, B. H., Tappa, K. D., and Lohmann, K. C.: Comparisons of the ecology and stable isotopic compositions of living (stained) benthic foraminifera from the Sulu and South China Seas, Deep Sea Res. Pt. I, 43, 1617–1646, 1996.

Rebesco, M., Hernández-Molina, F. J., Van Rooij, D., and Wåhlin, A.: Contourites and associated sediments controlled by deep-water circulation processes: State-of-the-art and future considerations, Mar. Geol., 352, 111–154, https://doi.org/10.1016/j.margeo.2014.03.011, 2014.

Roberts, J. M. and Cairns, S. D.: Cold-water corals in a changing ocean, Curr. Opin. Env. Sust., 7, 118–126, https://doi.org/10.1016/j.cosust.2014.01.004, 2014.

Rohling, E., Foster, G. L., Grant, K., Marino, G., Roberts, A., Tamisiea, M. E., and Williams, F.: Sea-level and deep-sea-temperature variability over the past 5.3 million years, Nature, 508, 477–482, 2014.

Roughan, M. and Middleton, J. H.: A comparison of observed upwelling mechanisms off the east coast of Australia, Cont. Shelf Res., 22, 2551–2572, 2002.

Ruckelshausen, M.: Cold-water corals: A paleoceanographic archive; Tracing past ocean circulation changes in the mid-depth subtropical western South Atlantic off Brazil for the last 40 ka BP, PhD thesis, Heidelberg University, 215 pp., 2013.

Rüggeberg, A., Dorschel, B., Dullo, W.-C., and Hebbeln, D.: Sedimentary patterns in the vicinity of a carbonate mound in the Hovland Mound Province, northern Porcupine Seabight, in: Cold-water corals and ecosystems, edited by: Freiwald, A. and Roberts, J. M., Springer, Berlin, Heidelberg, 87–112, 2005.

Rüggeberg, A., Flögel, S., Dullo, W. C., Raddatz, J., and Liebetrau, V.: Paleoseawater density reconstruction and its implication for cold-water coral carbonate mounds in the northeast Atlantic through time, Paleoceanography, 31, 365–379, 2016.

Skornitzke, S., Raddatz, J., Bahr, A., Pahn, G., Kauczor, H.-U., and Stiller, W.: Experimental application of an automated alignment correction algorithm for geological CT imaging: phantom study and application to sediment cores from cold-water coral mounds, Eur. Radiol. Exp., 3, 12, https://doi.org/10.1186/s41747-019-0091-8, 2019.

Soetaert, K., Mohn, C., Rengstorf, A., Grehan, A., and Van Oevelen, D.: Ecosystem engineering creates a direct nutritional link between 600-m deep cold-water coral mounds and surface productivity, Sci. Rep., 6, 35057, https://doi.org/10.1038/srep35057, 2016.

Stalling, D., Westerhoff, M., and Hege, H.-C.: Amira: A highly interactive system for visual data analysis, The Visualization Handbook, 38, 749–767, 2005.

Stramma, L. and England, M.: On the water masses and mean circulation of the South Atlantic Ocean, J. Geophys. Res.-Oceans, 104, 20863–20883, 1999.

Stríkis, N. M., Chiessi, C. M., Cruz, F. W., Vuille, M., Cheng, H., Souza Barreto, E. A., Mollenhauer, G., Kasten, S., Karmann, I., and Edwards, R. L.: Timing and structure of Mega-SACZ events during Heinrich Stadial 1, Geophys. Res. Lett., 42, 5477–5484, 2015.

Stuut, J.-B. W., Prins, M. A., Schneider, R. R., Weltje, G. J., Jansen, J. F., and Postma, G.: A 300-kyr record of aridity and wind strength in southwestern Africa: inferences from grain-size distributions of sediments on Walvis Ridge, SE Atlantic, Mar. Geol., 180, 221–233, 2002.

Sumida, P. Y. G., Yoshinaga, M. Y., Madureira, L. A. S.-P., and Hovland, M.: Seabed pockmarks associated with deepwater corals off SE Brazilian continental slope, Santos Basin, Mar. Geol., 207, 159–167, 2004.

Sverdrup, H. U., Johnson, M. W., and Fleming, R. H.: The Oceans: Their physics, chemistry, and general biology, Prentice-Hall, New York, 1942.

Thiem, Ø., Ravagnan, E., Fosså, J. H., and Berntsen, J.: Food supply mechanisms for cold-water corals along a continental shelf edge, J. Marine Syst., 60, 207–219, 2006.

Theodor, M., Schmiedl, G., and Mackensen, A.: Stable isotope composition of deep-sea benthic foraminifera under contrasting trophic conditions in the western Mediterranean Sea, Mar. Micropaleontology, 124, 16–28, 2016.

Thresher, R. E., Tilbrook, B., Fallon, S., Wilson, N. C., and Adkins, J.: Effects of chronic low carbonate saturation levels on the distribution, growth and skeletal chemistry of deep-sea corals and other seamount megabenthos, Mar. Ecol. Prog. Ser., 442, 87–99, 2011.

Titschack, J., Thierens, M., Dorschel, B., Schulbert, C., Freiwald, A., Kano, A., Takashima, C., Kawagoe, N., Li, X., and Expedition, I.: Carbonate budget of a cold-water coral mound (Challenger Mound, IODP Exp. 307), Mar. Geol., 259, 36–46, 2009.

Titschack, J., Baum, D., De Pol-Holz, R., López Correa, M., Forster, N., Flögel, S., Hebbeln, D., and Freiwald, A.: Aggradation and carbonate accumulation of Holocene Norwegian cold-water coral reefs, Sedimentology, 62, 1873–1898, doi:10.1111/sed.12206, 2015.

Titschack, J., Fink, H. G., Baum, D., Wienberg, C., Hebbeln, D., and Freiwald, A.: Mediterranean cold-water corals–an important regional carbonate factory?, The Depositional Record, 2, 74–96, 2016.

Turnewitsch, R., Reyss, J.-L., Chapman, D. C., Thomson, J., and Lampitt, R. S.: Evidence for a sedimentary fingerprint of an asymmetric flow field surrounding a short seamount, Earth Planet. Sci. Lett., 222, 1023–1036, https://doi.org/10.1016/j.epsl.2004.03.042, 2004.

van Oevelen, D., Mueller, C. E., Lundälv, T., and Middelburg, J. J.: Food selectivity and processing by the cold-water coral Lophelia pertusa, Biogeosciences, 13, 5789–5798, https://doi.org/10.5194/bg-13-5789-2016, 2016.

Viana, A. and Faugères, J.-C.: Upper slope sand deposits: the example of Campos Basin, a latest Pleistocene-Holocene record of the interaction between alongslope and downslope currents, Geological Society, London, Special Publications, 129, 287–316, 1998.

Viana, A., Faugères, J., Kowsmann, R., Lima, J., Caddah, L., and Rizzo, J.: Hydrology, morphology and sedimentology of the Campos continental margin, offshore Brazil, Sediment. Geol., 115, 133–157, 1998.

Viana, A. R.: Seismic expression of shallow-to deep-water contourites along the south-eastern Brazilian margin, Mar. Geophys. Res., 22, 509–521, 2001.

Waelbroeck, C., Labeyrie, L., Michel, E., Duplessy, J. C., McManus, J. F., Lambeck, K., Balbon, E., and Labracherie, M.: Sea-level and deep water temperature changes derived from benthic foraminifera isotopic records, Quaternary Sci. Rev., 21, 295–305, 2002.

Waelbroeck, C., Pichat, S., Böhm, E., Lougheed, B. C., Faranda, D., Vrac, M., Missiaen, L., Vazquez Riveiros, N., Burckel, P., Lippold, J., Arz, H. W., Dokken, T., Thil, F., and Dapoigny, A.: Relative timing of precipitation and ocean circulation changes in the western equatorial Atlantic over the last 45 kyr, Clim. Past, 14, 1315–1330, https://doi.org/10.5194/cp-14-1315-2018, 2018.

Wang, X., Auler, A. S., Edwards, R. L., Cheng, H., Cristalli, P. S., Smart, P. L., Richards, D. A., and Shen, C.-C.: Wet periods in northeastern Brazil over the past 210 kyr linked to distant climate anomalies, Nature, 432, 740–743, doi:10.1038/nature03067, 2004.

Weaver, R.: Quartz presence in relationship to gibbsite stability in some highly weathered soils of Brazil, Clay. Clay Miner., 23, 431–436, 1975.

White, M., Wolff, G. A., Lundälv, T., Guihen, D., Kiriakoulakis, K., Lavaleye, M., and Duineveld, G.: Cold-water coral ecosystem (Tisler Reef, Norwegian Shelf) may be a hotspot for carbon cycling, Mar. Ecol. Prog. Ser., 465, 11–23, 2012.

Wienberg, C., Frank, N., Mertens, K. N., Stuut, J.-B., Marchant, M., Fietzke, J., Mienis, F., and Hebbeln, D.: Glacial cold-water coral growth in the Gulf of Cádiz: Implications of increased palaeoproductivity, Earth Planet. Sci. Lett., 298, 405–426, 2010.

Wienberg, C. and Titschack, J.: Framework-forming scleractinian cold-water corals through space and time: a late Quaternary North Atlantic perspective, in: Marine Animal Forests: The Ecology of Benthic Biodiversity Hotspots, edited by: Rossi, S., Bramanti, L., Gori, A., and Orejas Saco del Valle, C., Springer International Publishing, Cham, 699–732, 2017.

Wienberg, C., Titschack, J., Freiwald, A., Frank, N., Lundälv, T., Taviani, M., Beuck, L., Schröder-Ritzrau, A., Krengel, T., and Hebbeln, D.: The giant Mauritanian cold-water coral mound province: Oxygen control on coral mound formation, Quaternary Sci. Rev., 185, 135–152, 2018.

Wilson, M.: A study of weathering in a soil derived from a biotite-hornblende rock: I. Weathering of biotite, Clay Miner., 8, 291–303, 1970.

Zahn, R., Winn, K., and Sarnthein, J. M.: Benthic foraminiferal δ^{13}C and accumulation rates of organic carbon: *Uvigernina peregrina* group and *Cibicidoides wuellerstorfi*, Paleoceanography, 1, 27–42, 1986.